

LETTER

doi:10.1038/nature24471

A gravitational-wave standard siren measurement of the Hubble constant

The LIGO Scientific Collaboration and The Virgo Collaboration*, The 1M2H Collaboration*, The Dark Energy Camera GW-EM Collaboration and the DES Collaboration*, The DLT40 Collaboration*, The Las Cumbres Observatory Collaboration*, The VINROUGE Collaboration* & The MASTER Collaboration*

This is a PDF file of a peer-reviewed paper that has been accepted for publication. Although unedited, the content has been subjected to preliminary formatting. *Nature* is providing this early version of the typeset paper as a service to our customers. The text and figures will undergo copyediting and a proof review before the paper is published in its final form. Please note that during the production process errors may be discovered which could affect the content, and all legal disclaimers apply.

Cite this article as: Abbott, B. P. *et al.* A gravitational-wave standard siren measurement of the Hubble constant. *Nature* <http://dx.doi.org/10.1038/nature24471> (2017).

Received 26 September; accepted 5 October 2017.

Accelerated Article Preview Published online 16 October 2017.

A gravitational-wave standard siren measurement of the Hubble constant

The LIGO Scientific Collaboration and The Virgo Collaboration*, The 1M2H Collaboration*, The Dark Energy Camera GW-EM Collaboration and the DES Collaboration*, The DLT40 Collaboration*, The Las Cumbres Observatory Collaboration*, The VINROUGE Collaboration* & The MASTER Collaboration*

The detection of GW170817 (ref. 1) heralds the age of gravitational-wave multi-messenger astronomy, with the observations of gravitational-wave and electromagnetic emission from the same transient source. On 17 August 2017 the network of Advanced Laser Interferometer Gravitational-wave Observatory (LIGO)² and Virgo³ detectors observed GW170817, a strong signal from the merger of a binary neutron-star system. Less than two seconds after the merger, a γ -ray burst event, GRB 170817A, was detected consistent with the LIGO–Virgo sky localization region^{4–6}. The sky region was subsequently observed by optical astronomy facilities⁷, resulting in the identification of an optical transient signal within about 10 arcseconds of the galaxy NGC 4993 (refs 8–13). GW170817 can be used as a standard siren^{14–18}, combining the distance inferred purely from the gravitational-wave signal with the recession velocity arising from the electromagnetic data to determine the Hubble constant. This quantity, representing the local expansion rate of the Universe, sets the overall scale of the Universe and is of fundamental importance to cosmology. Our measurements do not require any form of cosmic ‘distance ladder’¹⁹; the gravitational-wave analysis directly estimates the luminosity distance out to cosmological scales. Here we report $H_0 = 70.0^{+12.0}_{-8.0}$ kilometres per second per megaparsec, which is consistent with existing measurements^{20,21}, while being completely independent of them.

The Hubble constant H_0 measures the mean expansion rate of the Universe. At nearby distances ($d \lesssim 50$ Mpc) it is well approximated by the expression

$$v_H = H_0 d \quad (1)$$

where v_H is the local ‘Hubble flow’ velocity of a source, and d is the distance to the source. At such distances all cosmological distance measures (such as luminosity distance and comoving distance) differ at the order of v_H/c where c is the speed of light. As $v_H/c \approx 1\%$ for GW170817 we do not distinguish between them. We are similarly insensitive to the values of other cosmological parameters, such as Ω_m and Ω_Λ .

To obtain the Hubble flow velocity at the position of GW170817, we use the optical identification of the host galaxy NGC 4993⁷. This identification is based solely on the two-dimensional projected offset and is independent of any assumed value of H_0 . The position and redshift of this galaxy allow us to estimate the appropriate value of the Hubble flow velocity. Because the source is relatively nearby the random relative motions of galaxies, known as peculiar velocities, need to be taken into account. The peculiar velocity is about 10% of the measured recessional velocity (see Methods).

The original standard siren proposal¹⁴ did not rely on the unique identification of a host galaxy. By combining information from around 100 independent gravitational-wave detections, each with a set of potential host galaxies, an approximately 5% estimate of H_0 can be

obtained even without the detection of any transient optical counterparts²². Alternatively, if an electromagnetic counterpart has been identified but the host galaxy is unknown, the same statistical method can be applied but using only those galaxies in a narrow beam around the location of the optical counterpart. However, such statistical analyses are sensitive to a number of complicating effects, including the incompleteness of current galaxy catalogs or the need for dedicated follow-up surveys, as well as a range of selection effects²³. In what follows we exploit the identification of NGC 4993 as the host galaxy of GW170817 to perform a standard siren measurement of the Hubble constant^{15–18}.

Analysis of the gravitational-wave data associated with GW170817 produces estimates for the parameters of the source, under the assumption that general relativity is the correct model of gravity¹. We are most interested in the joint posterior distribution on the luminosity distance and binary orbital inclination angle. For the analysis in this paper we fix the location of the gravitational-wave source on the sky to the identified location of the counterpart⁸. See Methods for details.

An analysis of the gravitational-wave data alone finds that GW170817 occurred at a distance $d = 43.8^{+2.9}_{-6.9}$ Mpc (all values are quoted as the maximum posterior value with the minimal width 68.3% credible interval). We note that the distance quoted here differs from that in other studies¹, since here we assume that the optical counterpart represents the true sky location of the gravitational-wave source instead of marginalizing over a range of potential sky locations. The approximately 15% uncertainty is due to a combination of statistical measurement error from the noise in the detectors, instrumental calibration uncertainties¹, and a geometrical factor dependent upon the correlation of distance with inclination angle. The gravitational-wave measurement is consistent with the distance to NGC 4993 measured using the Tully–Fisher relation, $d_{TF} = 41.1 \pm 5.8$ Mpc (refs 19, 24).

The measurement of the gravitational-wave polarization is crucial for inferring the binary inclination. This inclination, ι , is defined as the angle between the line of sight vector from the source to the detector and the orbital angular momentum vector of the binary system. For electromagnetic phenomena it is typically not possible to tell whether a system is orbiting clockwise or counter-clockwise (or, equivalently, face-on or face-off), and sources are therefore usually characterized by a viewing angle: $\min(\iota, 180^\circ - \iota)$. By contrast, gravitational-wave measurements can identify the sense of the rotation, and thus ι ranges from 0 (anticlockwise) to 180° (clockwise). Previous gravitational-wave detections by LIGO had large uncertainties in luminosity distance and inclination²⁵ because the two LIGO detectors that were involved are nearly co-aligned, preventing a precise polarization measurement. In the present case, thanks to Virgo as an additional detector, the cosine of the inclination can be constrained at 68.3% (1σ) confidence to the range $[-1.00, -0.81]$ corresponding to inclination angles between $[144^\circ, 180^\circ]$. This implies that the plane of the binary orbit is almost, but not quite, perpendicular to our line of sight to the source ($\iota \approx 180^\circ$),

*Lists of authors and their affiliations appear in the online version of the paper.

which is consistent with the observation of a coincident γ -ray burst^{4–6}. We report inferences on $\cos i$ because our prior for it is flat, so the posterior is proportional to the marginal likelihood for it from the gravitational-wave observations.

Electromagnetic follow-up of the gravitational-wave sky localization region⁷ discovered an optical transient^{8–12,26} in close proximity to the galaxy NGC 4993. The location of the transient was previously observed by the Distance Less Than 40 Mpc (DLT40) survey on 2017 July 27.99 UT and no sources were found¹⁰. We estimate the probability of a random chance association between the optical counterpart and NGC 4993 to be 0.004% (see Methods for details). In what follows we assume that the optical counterpart is associated with GW170817, and that this source resides in NGC 4993.

To compute H_0 we need to estimate the background Hubble flow velocity at the position of NGC 4993. In the traditional electromagnetic calibration of the cosmic ‘distance ladder’¹⁹, this step is commonly carried out using secondary distance indicator information, such as the Tully–Fisher relation²⁴, which allows one to infer the background Hubble flow velocity in the local Universe scaled back from more distant secondary indicators calibrated in quiet Hubble flow. We do not adopt this approach here, however, in order to preserve more fully the independence of our results from the electromagnetic distance ladder. Instead we estimate the Hubble flow velocity at the position of NGC 4993 by correcting for local peculiar motions.

NGC 4993 is part of a collection of galaxies, ESO-508, whose center-of-mass recession velocity relative to our local CMB frame²⁷ is²⁸ $3,327 \pm 72 \text{ km s}^{-1}$. We correct the group velocity by 310 km s^{-1} owing to the coherent bulk flow^{29,30} towards The Great Attractor (see Methods for details). The standard error on our estimate of the peculiar velocity is 69 km s^{-1} , but recognizing that this value may be sensitive to details of the bulk flow motion that have been imperfectly modelled, in our subsequent analysis we adopt a more conservative estimate³⁰ of 150 km s^{-1} for the uncertainty on the peculiar velocity at the location of NGC 4993, and fold this into our estimate of the uncertainty on v_H . From this, we obtain a Hubble velocity $v_H = 3,017 \pm 166 \text{ km s}^{-1}$.

Once the distance and Hubble velocity distributions have been determined from the gravitational-wave and electromagnetic data, respectively, we can constrain the value of the Hubble constant. The measurement of the distance is strongly correlated with the measurement of the inclination of the orbital plane of the binary. The analysis of the gravitational-wave data also depends on other parameters describing the source, such as the masses of the components²⁵. Here we treat the uncertainty in these other variables by marginalizing over the posterior distribution on system parameters¹, with the exception of the position of the system on the sky which is taken to be fixed at the location of the optical counterpart.

We carry out a Bayesian analysis to infer a posterior distribution on H_0 and inclination, marginalized over uncertainties in the recession and peculiar velocities; see the Methods section for details. Figure 1 shows the marginal posterior for H_0 . The maximum a posteriori value with the minimal 68.3% credible interval is $H_0 = 70.0^{+12.0}_{-8.0} \text{ km s}^{-1} \text{ Mpc}^{-1}$. Our estimate agrees well with state-of-the-art determinations of this quantity, including CMB measurements from Planck²⁰ ($67.74 \pm 0.46 \text{ km s}^{-1} \text{ Mpc}^{-1}$, ‘TT,TE,EE+lowP+lensing+ext’) and type Ia supernova measurements from SHoES²¹ ($73.24 \pm 1.74 \text{ km s}^{-1} \text{ Mpc}^{-1}$), as well as baryon acoustic oscillations measurements from SDSS³¹, strong lensing measurements from HOLiCOW³², high- l CMB measurements from SPT³³, and Cepheid measurements from the HST key project¹⁹. Our measurement is a new and independent determination of this quantity. The close agreement indicates that, although each method may be affected by different systematic uncertainties, we see no evidence at present for a systematic difference between gravitational-wave and established electromagnetic-based estimates. As has been much remarked upon, the Planck and SHoES results are inconsistent at $\gtrsim 3\sigma$ level. Our measurement does not resolve this tension, and is broadly consistent with both.

One of the main sources of uncertainty in our measurement of H_0 is due to the degeneracy between distance and inclination in the gravitational-wave measurements. A face-on or face-off binary far away has a similar amplitude to an edge-on binary closer in. This relationship is captured in Fig. 2, which shows posterior contours in the H_0 – $\cos i$ parameter space.

The posterior in Fig. 1 results from the vertical projection of Fig. 2, marginalizing out uncertainties in the cosine of inclination to derive constraints on the Hubble constant. Alternatively, it is possible to project horizontally, and thereby marginalize out the Hubble constant to derive constraints on the cosine of inclination. If instead of deriving H_0 independently we take the existing constraints on H_0 (refs 20, 21) as priors, we are able to significantly improve our constraints on $\cos i$ as shown in Fig. 3. Assuming the Planck value for H_0 , the minimal 68.3% credible interval for the cosine of inclination is $[-1.00, -0.92]$ (corresponding to an inclination angle range $[157^\circ, 177^\circ]$). For the SHoES value of H_0 , it is $[-0.97, -0.85]$ (corresponding to an inclination angle range $[148^\circ, 166^\circ]$). For this latter SHoES result we note that the face-off $i = 180^\circ$ orientation is just outside the 90% confidence range. It will be particularly interesting to compare these constraints to those from modeling of the short γ -ray burst, afterglow, and optical counterpart associated with GW170817 (ref. 7).

We have presented a standard siren determination of the Hubble constant, using a combination of a gravitational-wave distance and an electromagnetic Hubble velocity estimate. Our measurement does not use a ‘distance ladder’, and makes no prior assumptions about H_0 . We find $H_0 = 70.0^{+12.0}_{-8.0} \text{ km s}^{-1} \text{ Mpc}^{-1}$, which is consistent with existing measurements^{20,21}. This first gravitational-wave–electromagnetic multi-messenger event demonstrates the potential for cosmological inference from gravitational-wave standard sirens. The coming years can be expected to bring additional multi-messenger binary neutron star events, as well as numerous detections of binary black hole mergers²⁵, for which electromagnetic counterparts are not expected. Combining subsequent independent measurements of H_0 from these future standard sirens will only improve the estimate made from GW170817, leading to an era of percent-level gravitational-wave cosmology.

Online Content Methods, along with any additional Extended Data display items and Source Data, are available in the online version of the paper; references unique to these sections appear only in the online paper.

Received 26 September; accepted 5 October 2017.

Published online 16 October 2017.

- Abbott, B. P. *et al.* GW170817: observation of gravitational waves from a binary neutron star inspiral. *Phys. Rev. Lett.* <https://doi.org/10.1103/PhysRevLett.119.161101> (2017).
- The LIGO Scientific Collaboration. Advanced LIGO. *Class. Quantum Gravity* **32**, 074001 (2015).
- Acernese, F. *et al.* Advanced Virgo: a second-generation interferometric gravitational wave detector. *Class. Quantum Gravity* **32**, 024001 (2015).
- LVC GBM, & INTEGRAL, manuscript in preparation.
- Goldstein, A. *et al.* An ordinary short gamma-ray burst with extraordinary implications: Fermi-GBM detection of GRB 170817A. *Astrophys. J.* **848**, <https://doi.org/10.3847/2041-8213/aa8f41> (2017).
- Savchenko, V. *et al.* INTEGRAL detection of the first prompt gamma-ray signal coincident with the gravitational event GW170817. *Astrophys. J.* **848**, <https://doi.org/10.3847/2041-8213/aa8f94> (2017).
- Multi-messenger observations of a binary neutron star merger. *Astrophys. J.* **848**, <https://doi.org/10.3847/2041-8213/aa91c9> (2017).
- Coulter, D. A. *et al.* Swope Supernova Survey 2017a (SSS17a), the optical counterpart to a gravitational wave source. *Science* <http://doi.org/10.1126/science.aap9811> (2017).
- Soares-Santos, M. *et al.* The electromagnetic counterpart of the binary neutron star merger LIGO/VIRGO GW170817. I. Discovery of the optical counterpart using the dark energy camera. *Astrophys. J.* **848**, <https://doi.org/10.3847/2041-8213/aa9059> (2017).
- Valenti, S. *et al.* The discovery of the electromagnetic counterpart of GW170817: kilonova AT 2017gfo/DLT17ck. *Astrophys. J.* **848**, <https://doi.org/10.3847/2041-8213/aa8edf> (2017).
- Arcavi, I. *et al.* Optical emission from a kilonova following a gravitational-wave-detected neutron-star merger. *Nature* <http://doi.org/10.1038/nature24291> (2017).

12. Tanvir, N. *et al.* The emergence of a lanthanide-rich kilonova following the merger of two neutron stars. *Astrophys. J.* **848**, <https://doi.org/10.3847/2041-8213/aa90b6> (2017).
13. Lipunov, V. *et al.* MASTER optical detection of the first LIGO/Virgo NSs merging GW170817/G298048. *Astrophys. J.* (in the press).
14. Schutz, B. F. Determining the Hubble constant from gravitational wave observations. *Nature* **323**, 310–311 (1986).
15. Holz, D. E. & Hughes, S. A. Using gravitational-wave standard sirens. *Astrophys. J.* **629**, 15–22 (2005).
16. Dalal, N., Holz, D. E., Hughes, S. A. & Jain, B. Short GRB and binary black hole standard sirens as a probe of dark energy. *Phys. Rev. D* **74**, 063006 (2006).
17. Nissanke, S., Holz, D. E., Hughes, S. A., Dalal, N. & Sievers, J. L. Exploring short gamma-ray bursts as gravitational-wave standard sirens. *Astrophys. J.* **725**, 496–514 (2010).
18. Nissanke, S. *et al.* Determining the Hubble constant from gravitational wave observations of merging compact binaries. Preprint at <https://arxiv.org/abs/1307.2638> (2013).
19. Freedman, W. L. *et al.* Final results from the Hubble Space Telescope key project to measure the Hubble constant. *Astrophys. J.* **553**, 47–72 (2001).
20. Planck Collaboration. Planck 2015 results. XIII. Cosmological parameters. *Astron. Astrophys.* **594**, A13 (2016).
21. Riess, A. G. *et al.* A 2.4% determination of the local value of the Hubble constant. *Astrophys. J.* **826**, 56 (2016).
22. Del Pozzo, W. Inference of the cosmological parameters from gravitational waves: application to second generation interferometers. *Phys. Rev. D* **86**, 043011 (2012).
23. Messenger, C. & Veitch, J. Avoiding selection bias in gravitational wave astronomy. *New J. Phys.* **15**, 053027 (2013).
24. Sakai, S. *et al.* The Hubble Space Telescope key project on the extragalactic distance scale. XXIV. The calibration of Tully-Fisher relations and the value of the Hubble constant. *Astrophys. J.* **529**, 698–722 (2000).
25. Abbott, B. P. *et al.* Binary black hole mergers in the first Advanced LIGO observing run. *Phys. Rev. X* **6**, 041015 (2016).
26. Lipunov, V. *et al.* LIGO/Virgo G298048: MASTER observations of the NGC 4993. *GCN 21546* (2017).
27. Hinshaw, G. *et al.* Five-year Wilkinson microwave anisotropy probe observations: data processing, sky maps, and basic results. *Astrophys. J. Suppl. Ser.* **180**, 225–245 (2009).
28. Crook, A. C. *et al.* Groups of galaxies in the Two Micron All Sky Redshift Survey. *Astrophys. J.* **655**, 790–813 (2007); erratum **685**, 1320–1323 (2008).
29. Springob, C. M. *et al.* The 6dF Galaxy Survey: peculiar velocity field and cosmography. *Mon. Not. R. Astron. Soc.* **445**, 2677–2697 (2014).
30. Carrick, J., Turnbull, S. J., Lavaux, G. & Hudson, M. J. Cosmological parameters from the comparison of peculiar velocities with predictions from the $2M++$ density field. *Mon. Not. R. Astron. Soc.* **450**, 317–332 (2015).
31. Aubourg, É. *et al.* Cosmological implications of baryon acoustic oscillation measurements. *Phys. Rev. D* **92**, 123516 (2015).
32. Bonvin, V. *et al.* HOLICOW – V. New COSMOGRAIL time delays of HE 0435–1223: H_0 to 3.8 per cent precision from strong lensing in a flat Λ CDM model. *Mon. Not. R. Astron. Soc.* **465**, 4914–4930 (2017).
33. Henning, J. W. *et al.* Measurements of the temperature and E-mode polarization of the CMB from 500 square degrees of SPTpol data. Preprint at <https://arxiv.org/abs/1707.09353> (2017).

Acknowledgements We acknowledge the support of the United States National Science Foundation (NSF) for the construction and operation of the LIGO Laboratory and Advanced LIGO as well as the Science and Technology Facilities Council (STFC) of the United Kingdom, the Max-Planck-Society (MPS), and the State of Niedersachsen/Germany for support of the construction of Advanced LIGO and construction and operation of the GEO600 detector. Additional support for Advanced LIGO was provided by the Australian Research Council. We acknowledge the Italian Istituto Nazionale di Fisica Nucleare (INFN), the French Centre National de la Recherche Scientifique (CNRS) and the Foundation for Fundamental Research on Matter supported by the Netherlands Organisation for Scientific Research for the construction and operation of the Virgo detector and the creation and support of the EGO consortium. We acknowledge research support from these agencies as well as by the Council of Scientific and Industrial Research of India, the Department of Science and Technology, India, the Science and Engineering Research Board (SERB), India, the Ministry of Human Resource Development, India, the Spanish Agencia Estatal de Investigación, the Vicepresidència i Conselleria d'Innovació, Recerca i Turisme and the Conselleria d'Educació i Universitat del Govern de les Illes Balears, the Conselleria d'Educació, Investigació, Cultura i Esport de la Generalitat Valenciana, the National Science Centre of Poland, the Swiss National Science Foundation (SNSF), the Russian Foundation for Basic Research, the Russian Science Foundation, the European Commission, the European Regional Development Funds (ERDF), the Royal Society, the Scottish Funding Council, the Scottish Universities Physics Alliance, the Hungarian Scientific Research Fund (OTKA), the Lyon Institute of Origins (LIO), the National Research, Development and Innovation Office Hungary (NKFI), the National Research Foundation of Korea, Industry Canada and the Province of Ontario through the Ministry of Economic Development and Innovation, the Natural Science and Engineering Research Council Canada, the Canadian Institute for Advanced Research, the Brazilian Ministry of Science, Technology, Innovations, and Communications, the International Center for Theoretical Physics South

American Institute for Fundamental Research (ICTP-SAIFR), the Research Grants Council of Hong Kong, the National Natural Science Foundation of China (NSFC), the Leverhulme Trust, the Research Corporation, the Ministry of Science and Technology (MOST), Taiwan and the Kavli Foundation. We acknowledge the support of the NSF, STFC, MPS, INFN, CNRS and the State of Niedersachsen/Germany for provision of computational resources. This paper has been assigned the document number LIGO-P1700296. We thank the University of Copenhagen, DARK Cosmology Centre, and the Niels Bohr International Academy for hosting D.A.C., R.J.F., A.M.B., E.R. and M.R.S. during the discovery of GW170817/SSS17a. R.J.F., A.M.B., E.R. and D.E.H. were participating in the Kavli Summer Program in Astrophysics, 'Astrophysics with gravitational wave detections'. This program was supported by the the Kavli Foundation, Danish National Research Foundation, the Niels Bohr International Academy, and the DARK Cosmology Centre. The UCSC group is supported in part by NSF grant AST-1518052, the Gordon & Betty Moore Foundation, the Heising-Simons Foundation, generous donations from many individuals through a UCSC Giving Day grant, and from fellowships from the Alfred P. Sloan Foundation (R.J.F.), the David and Lucile Packard Foundation (R.J.F. and E.R.) and the Niels Bohr Professorship from the DNRF (E.R.). A.M.B. acknowledges support from a UCMEXUS-CONACYT Doctoral Fellowship. Support for this work was provided by NASA through Hubble Fellowship grants HST-HF-51348.001 and HST-HF-51373.001 awarded by the Space Telescope Science Institute, which is operated by the Association of Universities for Research in Astronomy, Inc., for NASA, under contract NAS5-26555. The Berger Time-Domain Group at Harvard is supported in part by the NSF through grants AST-1411763 and AST-1714498, and by NASA through grants NNX15AE50G and NNX16AC22G. Funding for the DES Projects has been provided by the DOE and NSF (USA), MEC/MICINN/MINECO (Spain), STFC (UK), HEFCE (UK), NCSA (UIUC), KICP (U. Chicago), CCAPP (Ohio State), MIFPA (Texas A&M), CNPQ, FAPERJ, FINEP (Brazil), DFG (Germany) and the Collaborating Institutions in the Dark Energy Survey. The Collaborating Institutions are Argonne Lab, UC Santa Cruz, University of Cambridge, CIEMAT-Madrid, University of Chicago, University College London, DES-Brazil Consortium, University of Edinburgh, ETH Zürich, Fermilab, University of Illinois, ICE (IEEC-CSIC), IFAE Barcelona, Lawrence Berkeley Lab, LMU München and the associated Excellence Cluster Universe, University of Michigan, NOAO, University of Nottingham, Ohio State University, University of Pennsylvania, University of Portsmouth, SLAC National Lab, Stanford University, University of Sussex, Texas A&M University and the OzDES Membership Consortium. Based in part on observations at Cerro Tololo Inter-American Observatory, National Optical Astronomy Observatory, which is operated by the Association of Universities for Research in Astronomy (AURA) under a cooperative agreement with the National Science Foundation. The DES Data Management System is supported by the NSF under grant numbers AST-1138766 and AST-1536171. The DES participants from Spanish institutions are partially supported by MINECO under grants AYA2015-71825, ESP2015-88861, FPA2015-68048, and Centro de Excelencia SEV-2012-0234, SEV-2016-0597 and MDM-2015-0509. Research leading to these results has received funding from the ERC under the European Union's Seventh Framework Programme including grants ERC 240672, 291329 and 306478. We acknowledge support from the Australian Research Council Centre of Excellence for All-sky Astrophysics (CAASTRO), through project number CE110001020. This manuscript has been authored by Fermi Research Alliance, LLC under contract number DE-AC02-07CH11359 with the US Department of Energy, Office of Science, Office of High Energy Physics. The United States Government retains and the publisher, by accepting the article for publication, acknowledges that the United States Government retains a non-exclusive, paid-up, irrevocable, world-wide license to publish or reproduce the published form of this manuscript, or allow others to do so, for United States Government purposes. D.J.S. acknowledges support for the DLT40 programme from NSF grant AST-1517649. Support for I.A. was provided by NASA through the Einstein Fellowship Program, grant PF6-170148. G.H., D.A.H. and C.M. are supported by NSF grant AST-1313484. D.P. acknowledges support by Israel Science Foundation grant 541/17. VINROUGE is an European Southern Observatory Large Survey (id: 0198.D-2010). MASTER acknowledges the Lomonosov MSU Development Programme and the Russian Federation Ministry of Education and Science. This research has made use of the NASA/IPAC Extragalactic Database (NED), which is operated by the Jet Propulsion Laboratory, California Institute of Technology, under contract with NASA.

Author Contributions All authors contributed to the work presented in this paper.

Author Information Reprints and permissions information is available at www.nature.com/reprints. The authors declare no competing financial interests. Readers are welcome to comment on the online version of the paper. Publisher's note: Springer Nature remains neutral with regard to jurisdictional claims in published maps and institutional affiliations. Correspondence and requests for materials should be addressed to The LIGO Scientific Collaboration (lsc-spokesperson@ligo.org) and The Virgo Collaboration (virgo-spokesperson@ego-gw.eu).

Reviewer Information *Nature* thanks N. Suntzeff and the other anonymous reviewer(s) for their contribution to the peer review of this work.

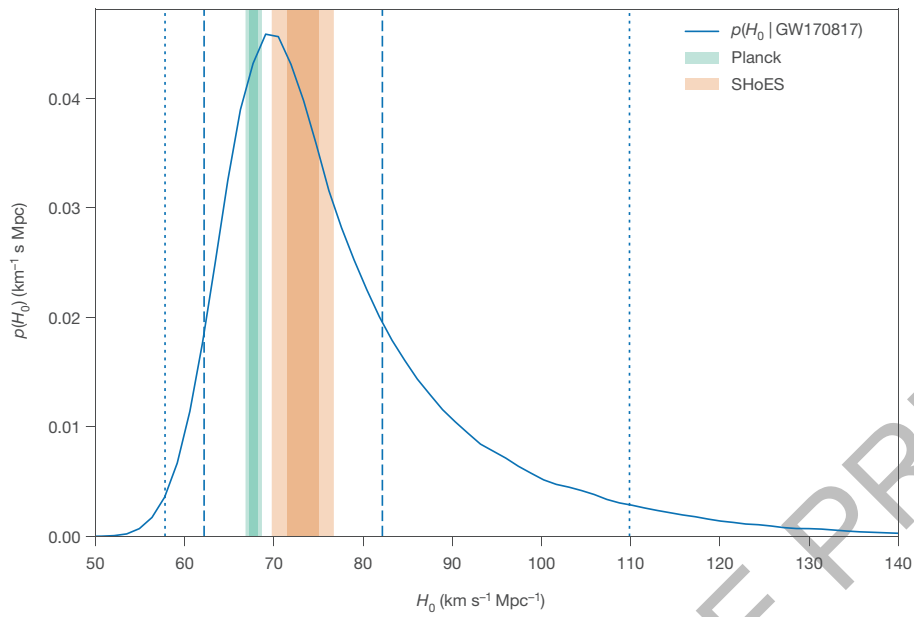


Figure 1 | GW170817 measurement of H_0 . Marginalized posterior density for H_0 (blue curve). Constraints at 1σ and 2σ from Planck²⁰ and SHoES²¹ are shown in green and orange. The maximum a posteriori value

and minimal 68.3% credible interval from this PDF is $H_0 = 70.0^{+12.0}_{-8.0} \text{ km s}^{-1} \text{Mpc}^{-1}$. The 68.3% (1σ) and 95.4% (2σ) minimal credible intervals are indicated by dashed and dotted lines.

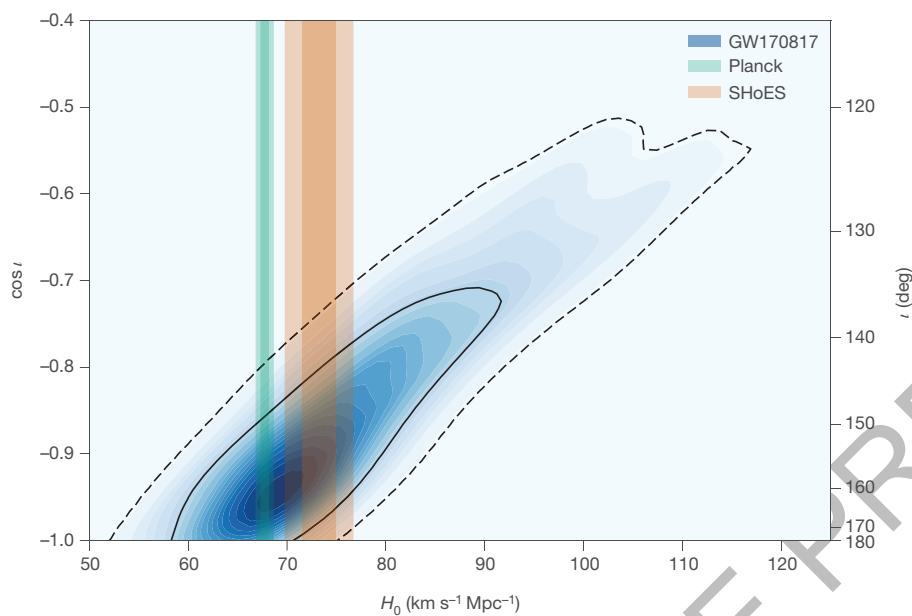


Figure 2 | Inference on H_0 and inclination. Posterior density of H_0 and $\cos i$ from the joint gravitational-wave–electromagnetic analysis (blue contours). Shading levels are drawn at every 5% credible level, with the 68.3% (1σ , solid) and 95.4% (2σ , dashed) contours in black. Values of H_0

and 1σ and 2σ error bands are also displayed from Planck²⁰ and SHoES²¹. As noted in the text, inclination angles near 180° ($\cos i = -1$) indicate that the orbital angular momentum is anti-parallel with the direction from the source to the detector.

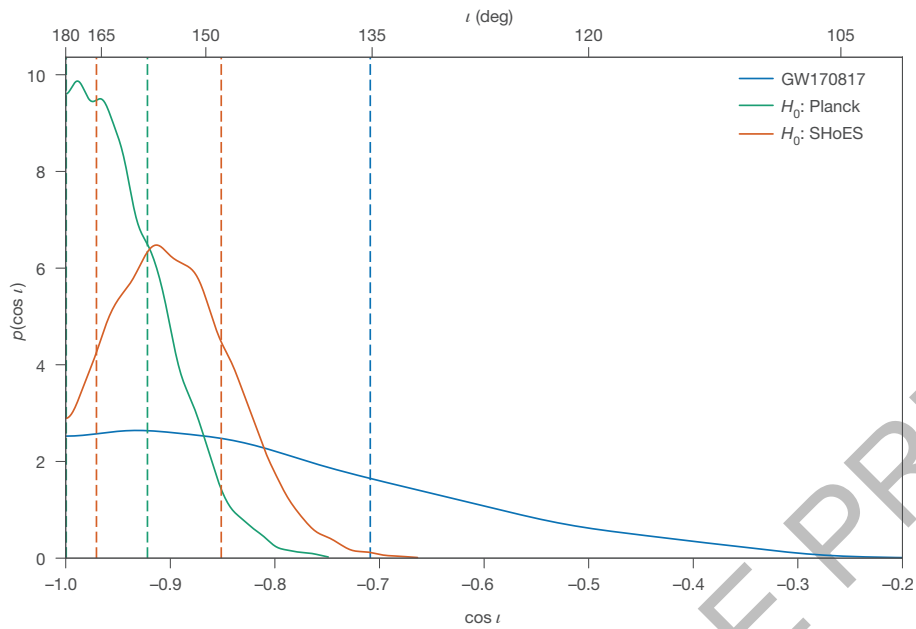


Figure 3 | Constraints on the inclination angle of GW170817. Posterior density on $\cos i$, for various assumptions about the prior distribution of H_0 . The analysis of the joint gravitational-wave and electromagnetic data with a $1/H_0$ prior density gives the blue curve; using values of H_0 from Planck²⁰ and SHoES²¹ as a prior on H_0 give the green and red curves, respectively. Choosing a narrow prior on H_0 converts the precise Hubble velocity

measurements for the group containing NGC 4993 to a precise distance measurement, breaking the distance inclination degeneracy, and leading to strong constraints on the inclination. Minimal 68.3% (1σ) credible intervals are indicated by dashed lines. Because our prior on inclination is flat on $\cos i$, the densities in this plot are proportional to the marginalised likelihood for $\cos i$.

J. H. Romie⁷, D. Rosińska^{150,56}, M. P. Ross¹⁵¹, S. Rowan⁴⁶, A. Rüdiger¹⁰, P. Ruggi³⁰, G. Rutins²⁷, K. Ryan⁴⁷, S. Sachdev¹, T. Sadecki⁴⁷, L. Sadeghian²¹, M. Sakellariadou¹⁵², L. Salconi³⁰, M. Saleem¹¹⁶, F. Salemi¹⁰, A. Samajdar¹⁴³, L. Sammut⁶, L. M. Sampson⁸⁹, E. J. Sanchez¹, L. E. Sanchez¹, N. Sanchis-Gual⁸⁵, V. Sandberg⁴⁷, J. R. Sanders⁴⁴, B. Sassolas²⁶, B. S. Sathyaprakash^{63,36}, P. R. Saulson⁴⁴, O. Sauter¹¹⁸, R. L. Savage⁴⁷, A. Sawadsky³⁴, P. Schale⁶⁹, M. Scheel⁴⁸, J. Scheuer⁸⁹, J. Schmidt¹⁰, P. Schmidt¹⁶⁵, R. Schnabel³⁴, R. M. S. Schofield⁶⁹, A. Schönbeck³⁴, E. Schreiber¹⁰, D. Schuette^{10,22}, B. W. Schulte¹⁰, B. F. Schutz^{36,10}, S. G. Schwab³⁷, J. Scott⁴⁶, S. M. Scott²⁵, E. Seidel¹², D. Sellers⁷, A. S. Sengupta¹⁵³, D. Sentenac³⁰, V. Sequino^{32,33,17}, A. Sergeev²⁸, D. A. Shaddock²⁵, T. J. Shaffer⁴⁷, A. A. Shah¹³⁷, M. S. Shahriar⁸⁹, M. B. Shaner¹⁰⁹, L. Shao³⁸, B. Shapiro⁵¹, P. Shawhan⁷⁵, A. Sheperd²¹, D. H. Shoemaker¹⁵, D. M. Shoemaker⁷⁶, K. Siellez⁷⁶, X. Siemens²¹, M. Sieniawska⁵⁶, D. Sigg⁴⁷, A. D. Silva¹⁶, L. P. Singer⁷⁹, A. Singh^{38,10,22}, A. Singhal^{17,35}, A. M. Sintal¹⁰², B. J. J. Slagmolen²⁵, B. Smith⁷, J. R. Smith²⁹, R. J. E. Smith¹⁶, S. Somala¹⁵⁴, E. J. Son¹³¹, J. A. Sonnenberg²¹, B. Sorazu⁴⁶, F. Sorrentino⁵⁹, T. Souradeep¹⁹, A. P. Spencer⁴⁶, A. K. Srivastava¹⁰⁵, K. Staats³⁷, A. Staley⁵⁰, D. Steer³⁹, M. Steinke¹⁰, J. Steinlechner^{34,46}, S. Steinlechner³⁴, D. Steinmeyer¹⁰, S. P. Stevenson^{58,149}, R. Stone¹⁰³, D. J. Stops⁵⁸, K. A. Strain⁴⁶, G. Stratta^{121,122}, S. E. Strigin⁶¹, A. Strunk⁴⁷, R. Sturani¹⁵⁵, A. L. Stuver⁷, T. Z. Summerscales¹⁵⁶, L. Sun⁹⁶, S. Sunil¹⁰⁵, J. Suresh¹⁹, P. J. Sutton³⁷, B. D. Swinkles³⁰, M. J. Szczepańczyk³⁷, M. Tacca¹⁴, S. C. Tait⁴⁶, C. Talbot⁶, D. Talukder⁶⁹, D. B. Tanner⁵, M. Tápai¹¹⁷, A. Taracchini³⁸, J. D. Tasson⁷¹, J. A. Taylor¹³⁷, R. Taylor¹, S. V. Tewari¹⁴⁸, T. Theeg¹⁰, F. Thies¹⁰, E. G. Thomas⁵⁸, M. Thomas⁷, P. Thomas⁴⁷, K. A. Thorne⁷, E. Thrane⁶, S. Tiwari^{17,95}, V. Tiwari³⁶, K. V. Tokmakov⁶², K. Toland⁴⁶, M. Tonelli^{23,24}, Z. Tornasi⁴⁶, A. Torres-Forné⁸⁵, C. I. Torrie¹, D. Tóyrás⁵⁸, F. Travasso^{30,43}, G. Traylor⁷, J. Tringali^{110,95}, M. C. Tringali^{110,95}, L. Trozzo^{157,24}, K. W. Tsang¹⁴, M. Tse¹⁵, R. Tso¹, L. Tsukada⁸¹, D. Tsuna⁸¹, D. Tuyenbayev¹⁰³, K. Ueno²¹, D. Ugolini¹⁵⁸, C. S. Unnikrishnan¹¹⁹, A. L. Urban¹, S. A. Usman³⁶, H. Vahlbruch²², G. Vajente¹, G. Valdes², N. van Bakel¹⁴, M. van Beuzekom¹⁴, J. F. J. van den Brand^{74,14}, C. Van Den Broeck¹⁴, D. C. VanderHyde⁴⁴, L. van der Schaaf¹⁴, J. V. van Heijningen¹⁴, A. A. van Veggel⁴⁶, M. Vardaro^{53,54}, V. Varma⁴⁸, S. Vass¹, M. Vasúth⁴⁹, A. Vecchio⁵⁸, G. Vedovato⁵⁴, J. Veitch⁴⁶, P. J. Veitch⁷², K. Venkateswara¹⁵¹, G. Venugopalan¹, D. Verkindt⁸, F. Vetruno^{121,122}, A. Viceré^{121,122}, A. D. Viets²¹, S. Vinciguerra⁵⁸, D. J. Vine²⁷, J.-Y. Vinet⁶⁶, S. Vitale¹⁵, T. Vo⁴⁴, H. Vocca^{42,43}, C. Vorvick⁴⁷, S. P. Vyatchanin⁶¹, A. R. Wade¹, L. E. Wade⁸⁴, M. Wade⁸⁴, R. Walet¹⁴, M. Walker²⁹, L. Wallace¹, S. Walsh^{38,10,21}, G. Wang^{17,122}, H. Wang⁵⁸, J. Z. Wang⁵³, W. H. Wang¹⁰³, Y. F. Wang⁹³, R. L. Ward²⁵, J. Warner⁴⁷, M. Was⁸, J. Watchi⁹⁸, B. Weaver⁴⁷, L.-W. Wei^{10,22}, M. Weinert¹⁰, A. J. Weinstein¹, R. Weiss¹⁵, L. Wen⁶⁴, E. K. Wessel¹², P. Weßels¹⁰, J. Westerweck¹⁰, T. Westphal¹⁰, K. Wette²⁵, J. T. Whelan⁵⁷, S. E. Whitcomb¹, B. F. Whiting⁵, C. Whittle⁶, D. Wilken¹⁰, D. Williams⁴⁶, R. D. Williams¹, A. R. Williamson⁶⁵, J. L. Willis¹⁵⁹, B. Wilke^{22,10}, M. H. Wimmer¹⁰, W. Winkler¹⁰, C. C. Wipf¹, H. Wittel^{10,22}, G. Woan⁴⁶, J. Woehler¹⁰, J. Wofford⁵⁷, K. W. K. Wong⁹³, J. Worden⁴⁷, J. L. Wright⁴⁶, D. S. Wu¹⁰, D. M. Wysocki⁵⁷, S. Xiao¹, H. Yamamoto¹, C. C. Yancey⁷⁵, L. Yang¹⁶⁰, M. J. Yap²⁵, M. Yazback⁵⁵, Hang Yu¹⁵, Haocun Yu¹⁵, M. Yvert⁸, A. Zadrozny¹³², M. Zanolin³⁷, T. Zelenova³⁰, J.-P. Zeng⁵⁴, M. Zevin⁸⁹, L. Zhang¹, M. Zhang¹⁴⁰, T. Zhang⁴⁶, Y.-H. Zhang⁵⁷, C. Zhao⁶⁴, M. Zhou⁸⁹, Z. Zhou⁸⁹, S. J. Zhu^{38,10}, X. J. Zhu⁶, A. B. Zimmerman⁹⁰, M. E. Zucker^{1,15} & J. Zweigig¹

¹LIGO, California Institute of Technology, Pasadena, California 91125, USA. ²Louisiana State University, Baton Rouge, Louisiana 70803, USA. ³Università di Salerno, Fisciano, I-84084 Salerno, Italy. ⁴INFN, Sezione di Napoli, Complesso Universitario di Monte S. Angelo, I-80126 Napoli, Italy. ⁵University of Florida, Gainesville, Florida 32611, USA. ⁶OzGrav, School of Physics and Astronomy, Monash University, Clayton, Victoria 3800, Australia. ⁷LIGO Livingston Observatory, Livingston, Louisiana 70754, USA. ⁸Laboratoire d'Annecy-le-Vieux de Physique des Particules (LAPP), Université Savoie Mont Blanc, CNRS/IN2P3, F-74941 Annecy, France. ⁹University of Sannio at Benevento, I-82100 Benevento, Italy and INFN, Sezione di Napoli, I-80100 Napoli, Italy. ¹⁰Max Planck Institute for Gravitational Physics (Albert Einstein Institute), D-30167 Hannover, Germany. ¹¹The University of Mississippi, University, Mississippi 38677, USA. ¹²NCSA, University of Illinois at Urbana-Champaign, Urbana, Illinois 61801, USA. ¹³University of Cambridge, Cambridge CB2 1TN, UK. ¹⁴Nikhef, Science Park, 1098 XG Amsterdam, The Netherlands. ¹⁵LIGO, Massachusetts Institute of Technology, Cambridge, Massachusetts 02139, USA. ¹⁶Instituto Nacional de Pesquisas Espaciais, 12227-010 São José dos Campos, São Paulo, Brazil. ¹⁷Gran Sasso Science Institute (GSSI), I-67100 L'Aquila, Italy. ¹⁸INFN, Laboratori Nazionali del Gran Sasso, I-67100 Assergi, Italy. ¹⁹Inter-University Centre for Astronomy and Astrophysics, Pune 411007, India. ²⁰International Centre for Theoretical Sciences, Tata Institute of Fundamental Research, Bengaluru 560089, India. ²¹University of Wisconsin-Milwaukee, Milwaukee, Wisconsin 53201, USA. ²²Leibniz Universität Hannover, D-30167 Hannover, Germany. ²³Università di Pisa, I-56127 Pisa, Italy. ²⁴INFN, Sezione di Pisa, I-56127 Pisa, Italy. ²⁵OzGrav, Australian National University, Canberra, Australian Capital Territory 0200, Australia. ²⁶Laboratoire des Matériaux Avancés (LMA), CNRS/IN2P3, F-69622 Villeurbanne, France. ²⁷SUPA, University of the West of Scotland, Paisley PA1 2BE, UK. ²⁸LAL, Université Paris-Sud, CNRS/IN2P3, Université Paris-Saclay, F-91898 Orsay, France. ²⁹California State University Fullerton, Fullerton, California 92831, USA. ³⁰European Gravitational Observatory (EGO), I-56021 Cascina, Italy. ³¹Chennai Mathematical Institute, Chennai 603103, India. ³²Università di Roma Tor Vergata, I-00133 Roma, Italy. ³³INFN, Sezione di Roma Tor Vergata, I-00133 Roma, Italy. ³⁴Universität Hamburg, D-22761 Hamburg, Germany. ³⁵INFN, Sezione di Roma, I-00185 Roma, Italy.

³⁶Cardiff University, Cardiff CF24 3AA, UK. ³⁷Embry-Riddle Aeronautical University, Prescott, Arizona 86301, USA. ³⁸Max Planck Institute for Gravitational Physics (Albert Einstein Institute), D-14476 Potsdam-Golm, Germany. ³⁹APC, AstroParticule et Cosmologie, Université Paris Diderot, CNRS/IN2P3, CEA/Irfu, Observatoire de Paris, Sorbonne Paris Cité, F-75205 Paris Cedex 13, France. ⁴⁰Korea Institute of Science and Technology Information, Daejeon 34141, South Korea. ⁴¹West Virginia University, Morgantown, West Virginia 26506, USA. ⁴²Università di Perugia, I-06123 Perugia, Italy. ⁴³INFN, Sezione di Perugia, I-06123 Perugia, Italy. ⁴⁴Syracuse University, Syracuse, New York 13244, USA. ⁴⁵University of Minnesota, Minneapolis, Minnesota 55455, USA. ⁴⁶SUPA, University of Glasgow, Glasgow G12 8QQ, UK. ⁴⁷LIGO Hanford Observatory, Richland, Washington 99352, USA. ⁴⁸Caltech CaRT, Pasadena, California 91125, USA. ⁴⁹Wigner RCP, RMKI, Konkoly Thege Miklós út 29-33, H-1121 Budapest, Hungary. ⁵⁰Columbia University, New York, New York 10027, USA. ⁵¹Stanford University, Stanford, California 94305, USA. ⁵²Università di Camerino, Dipartimento di Fisica, I-62032 Camerino, Italy. ⁵³Università di Padova, Dipartimento di Fisica e Astronomia, I-35131 Padova, Italy. ⁵⁴INFN, Sezione di Padova, I-35131 Padova, Italy. ⁵⁵Institute of Physics, Eötvös University, Pázmány P. s. 1/A, Budapest 1117, Hungary. ⁵⁶Nicolaus Copernicus Astronomical Center, Polish Academy of Sciences, 00-716 Warsaw, Poland. ⁵⁷Rochester Institute of Technology, Rochester, New York 14623, USA. ⁵⁸University of Birmingham, Birmingham B15 2TT, UK. ⁵⁹INFN, Sezione di Genova, I-16146 Genova, Italy. ⁶⁰RRCAT, Indore MP 452013, India. ⁶¹Faculty of Physics, Lomonosov Moscow State University, Moscow 119991, Russia. ⁶²SUPA, University of Strathclyde, Glasgow G1 1XQ, UK. ⁶³The Pennsylvania State University, University Park, Pennsylvania 16802, USA. ⁶⁴OzGrav, University of Western Australia, Crawley, Western Australia 6009, Australia. ⁶⁵Department of Astrophysics/IMAPP, Radboud University Nijmegen, PO Box 9010, 6500 GL Nijmegen, The Netherlands. ⁶⁶Artemis, Université Côte d'Azur, Observatoire Côte d'Azur, CNRS, CS 34229, F-06304 Nice Cedex 4, France. ⁶⁷Institut FOTON, CNRS, Université de Rennes 1, F-35042 Rennes, France. ⁶⁸Washington State University, Pullman, Washington 99164, USA. ⁶⁹University of Oregon, Eugene, Oregon 97403, USA. ⁷⁰Laboratoire Kastler Brossel, UPMC-Sorbonne Universités, CNRS, ENS-PSL Research University, Collège de France, F-75005 Paris, France. ⁷¹Carleton College, Northfield, Minnesota 55057, USA. ⁷²OzGrav, University of Adelaide, Adelaide, South Australia 5005, Australia. ⁷³Astronomical Observatory Warsaw University, 00-478 Warsaw, Poland. ⁷⁴VU University Amsterdam, 1081 HV Amsterdam, The Netherlands. ⁷⁵University of Maryland, College Park, Maryland 20742, USA. ⁷⁶Center for Relativistic Astrophysics, Georgia Institute of Technology, Atlanta, Georgia 30332, USA. ⁷⁷Université Claude Bernard Lyon 1, F-69622 Villeurbanne, France. ⁷⁸Università di Napoli 'Federico II', Complesso Universitario di Monte S. Angelo, I-80126 Napoli, Italy. ⁷⁹NASA Goddard Space Flight Center, Greenbelt, Maryland 20771, USA. ⁸⁰Dipartimento di Fisica, Università degli Studi di Genova, I-16146 Genova, Italy. ⁸¹RESCEU, University of Tokyo, Tokyo 113-0033, Japan. ⁸²Tsinghua University, Beijing 100084, China. ⁸³Texas Tech University, Lubbock, Texas 79409, USA. ⁸⁴Kenyon College, Gambier, Ohio 43022, USA. ⁸⁵Departamento de Astronomía y Astrofísica, Universidad de València, E-46100 Burjassot, Spain. ⁸⁶Museo Storico della Fisica e Centro Studi e Ricerche Enrico Fermi, I-00184 Roma, Italy. ⁸⁷National Tsing Hua University, Hsinchu City, 30013 Taiwan, China. ⁸⁸Charles Sturt University, Wagga Wagga, New South Wales 2678, Australia. ⁸⁹Center for Interdisciplinary Exploration and Research in Astrophysics (CIERA), Northwestern University, Evanston, Illinois 60208, USA. ⁹⁰Canadian Institute for Theoretical Astrophysics, University of Toronto, Toronto, Ontario M5S 3H8, Canada. ⁹¹University of Chicago, Chicago, Illinois 60637, USA. ⁹²Pusan National University, Busan 46241, South Korea. ⁹³The Chinese University of Hong Kong, Shatin, Hong Kong. ⁹⁴INFN, Osservatorio Astronomico di Padova, I-35122 Padova, Italy. ⁹⁵INFN, Trento Institute for Fundamental Physics and Applications, I-38123 Povo, Italy. ⁹⁶OzGrav, University of Melbourne, Parkville, Victoria 3010, Australia. ⁹⁷Università di Roma 'La Sapienza', I-00185 Roma, Italy. ⁹⁸Université Libre de Bruxelles, 1050 Brussels, Belgium. ⁹⁹Sonoma State University, Rohnert Park, California 94928, USA. ¹⁰⁰Departamento de Matemáticas, Universidad de València, E-46100 Burjassot, Spain. ¹⁰¹Montana State University, Bozeman, Montana 59717, USA. ¹⁰²Université de les Illes Balears, IAC3—IEEC, E-07122 Palma de Mallorca, Spain. ¹⁰³The University of Texas Rio Grande Valley, Brownsville, Texas 78520, USA. ¹⁰⁴Bellevue College, Bellevue, Washington 98007, USA. ¹⁰⁵Institute for Plasma Research, Bhat, Gandhinagar 382428, India. ¹⁰⁶The University of Sheffield, Sheffield S10 2TN, UK. ¹⁰⁷Dipartimento di Scienze Matematiche, Fisiche e Informatiche, Università di Parma, I-43124 Parma, Italy. ¹⁰⁸INFN, Sezione di Milano Bicocca, Gruppo Collegato di Parma, I-43124 Parma, Italy. ¹⁰⁹California State University, Los Angeles, 5151 State University Drive, Los Angeles, California 90032, USA. ¹¹⁰Università di Trento, Dipartimento di Fisica, I-38123 Povo, Italy. ¹¹¹Montclair State University, Montclair, New Jersey 07043, USA. ¹¹²National Astronomical Observatory of Japan, 2-21-1 Osawa, Mitaka, Tokyo 181-8588, Japan. ¹¹³Osservatorio Astronomico, Universidad de València, E-46980 Paterna, Spain. ¹¹⁴School of Mathematics, University of Edinburgh, Edinburgh EH9 3FD, UK. ¹¹⁵University and Institute of Advanced Research, Koba Institutional Area, Gandhinagar Gujarat 382007, India. ¹¹⁶IISER-TVM, CET Campus, Trivandrum Kerala 695016, India. ¹¹⁷University of Szeged, Dóm tér 9, 6720 Szeged, Hungary. ¹¹⁸University of Michigan, Ann Arbor, Michigan 48109, USA. ¹¹⁹Tata Institute of Fundamental Research, Mumbai 400005, India. ¹²⁰INFN, Osservatorio Astronomico di Capodimonte, I-80131 Napoli, Italy. ¹²¹Università degli Studi di Urbino 'Carlo Bo', I-61029 Urbino, Italy. ¹²²INFN, Sezione di Firenze, I-50019 Sesto Fiorentino, Italy. ¹²³Physik-Institut, Universität of Zurich, Winterthurerstrasse 190, 8057 Zurich, Switzerland. ¹²⁴American University, Washington DC 20016, USA. ¹²⁵University of Białystok, 15-424 Białystok, Poland. ¹²⁶University of Southampton, Southampton SO17 1BJ, UK. ¹²⁷University of Washington Bothell, 18115 Campus Way NE, Bothell, Washington 98011, USA. ¹²⁸Institute of Applied Physics, Nizhny Novgorod 603950, Russia. ¹²⁹Korea Astronomy and Space Science Institute, Daejeon 34055, South Korea. ¹³⁰Inje University Gimhae, South Gyeongsang 50834, South Korea. ¹³¹National Institute for Mathematical Sciences, Daejeon 34047, South Korea. ¹³²NCBJ, 05-400 Swierk-Otwock, Poland.

¹³³Institute of Mathematics, Polish Academy of Sciences, 00656 Warsaw, Poland. ¹³⁴Hillsdale College, Hillsdale, Michigan 49242, USA. ¹³⁵Hanyang University, Seoul 04763, South Korea. ¹³⁶Seoul National University, Seoul 08826, South Korea. ¹³⁷NASA Marshall Space Flight Center, Huntsville, Alabama 35811, USA. ¹³⁸ESPCI, CNRS, F-75005 Paris, France. ¹³⁹Southern University and A&M College, Baton Rouge, Louisiana 70813, USA. ¹⁴⁰College of William and Mary, Williamsburg, Virginia 23187, USA. ¹⁴¹Centre Scientifique de Monaco, 8 quai Antoine Ier, MC-98000, Monaco. ¹⁴²Indian Institute of Technology Madras, Chennai 600036, India. ¹⁴³IISER-Kolkata, Mohanpur, West Bengal 741252, India. ¹⁴⁴Whitman College, 345 Boyer Avenue, Walla Walla, Washington 99362 USA. ¹⁴⁵Indian Institute of Technology Bombay, Powai, Mumbai, Maharashtra 400076, India. ¹⁴⁶Scuola Normale Superiore, Piazza dei Cavalieri 7, I-56126 Pisa, Italy. ¹⁴⁷Université de Lyon, F-69361 Lyon, France. ¹⁴⁸Hobart and William Smith Colleges, Geneva, New York 14456, USA. ¹⁴⁹OzGrav, Swinburne University of Technology, Hawthorn, Victoria 3122, Australia. ¹⁵⁰Janusz Gil Institute of Astronomy, University of Zielona Góra, 65-265 Zielona Góra, Poland. ¹⁵¹University of Washington, Seattle, Washington 98195, USA. ¹⁵²King's College London, University of London, London WC2R 2LS, UK. ¹⁵³Indian Institute of Technology, Gandhinagar Ahmedabad Gujarat 382424, India. ¹⁵⁴Indian Institute of Technology Hyderabad, Sangareddy, Khandi, Telangana 502285, India. ¹⁵⁵International Institute of Physics, Universidade Federal do Rio Grande do Norte, Natal RN 59078-970, Brazil. ¹⁵⁶Andrews University, Berrien Springs, Michigan 49104, USA. ¹⁵⁷Università di Siena, I-53100 Siena, Italy. ¹⁵⁸Trinity University, San Antonio, Texas 78212, USA. ¹⁵⁹Abilene Christian University, Abilene, Texas 79699, USA. ¹⁶⁰Colorado State University, Fort Collins, Colorado 80523, USA.

The 1M2H Collaboration

R. J. Foley¹, D. A. Coulter¹, M. R. Drout^{2,3}, D. Kasen^{4,5}, C. D. Kilpatrick¹, B. F. Madore², A. Murguía-Berthier¹, Y.-C. Pan¹, A. L. Piro², J. X. Prochaska¹, E. Ramirez-Ruiz^{1,6}, A. Rest⁷, C. Rojas-Bravo¹, B. J. Shappee^{2,8,9}, M. R. Siebert¹, J. D. Simon² & N. Ulloa¹⁰

¹Department of Astronomy and Astrophysics, University of California, Santa Cruz, California 95064, USA. ²The Observatories of the Carnegie Institution for Science, 813 Santa Barbara Street, Pasadena, California 91101, USA. ³Hubble and Carnegie-Dunlap Fellow. ⁴Nuclear Science Division, Lawrence Berkeley National Laboratory, Berkeley, California 94720, USA. ⁵Departments of Physics and Astronomy, University of California, Berkeley, California 94720, USA. ⁶Dark Cosmology Centre, Niels Bohr Institute, University of Copenhagen, Blegdamsvej 17, 2100 Copenhagen, Denmark. ⁷Space Telescope Science Institute, 3700 San Martin Drive, Baltimore, Maryland 21218, USA. ⁸Institute for Astronomy, University of Hawaii, 2680 Woodlawn Drive, Honolulu, Hawaii 96822, USA. ⁹Hubble and Carnegie-Princeton Fellow. ¹⁰Departamento de Física y Astronomía, Universidad de La Serena, La Serena, Chile.

The Dark Energy Camera GW-EM Collaboration and The DES Collaboration

J. Annis¹, M. Soares-Santos^{2,1}, D. Brout³, D. Scolnic⁴, H. T. Diehl¹, J. Frieman^{1,4}, E. Berger⁵, K. D. Alexander⁵, S. Allam¹, E. Balbinot⁶, P. Blanchard⁷, R. E. Butler^{8,1}, R. Chornock⁹, E. R. Cook^{10,11}, P. Cowperthwaite⁵, A. Drica-Wagner¹, M. R. Drout^{12,13}, T. Durret¹⁴, T. Eftekhari¹, D. A. Finley¹, W. Fong^{15,16}, C. L. Fryer¹⁷, J. García-Bellido¹⁸, M. S.S. Gill¹⁹, R. A. Gruendl^{20,21}, C. Hanna^{22,21}, W. Hartley^{23,24}, K. Herner¹, D. Huterer²⁵, D. Kasen²⁶, R. Kessler⁴, T. S. Li¹, H. Lin¹, P. A. A. Lopes²⁷, A. C. C. Lourenço²⁷, R. Margutti²⁸, J. Marriner¹, J. L. Marshall¹⁰, T. Matheson²⁹, G. E. Medina³⁰, B. D. Metzger³¹, R. R. Muñoz³⁰, J. Muir³², M. Nicholl⁵, P. Nugent³³, A. Palmese²³, F. Paz-Chinchón²¹, E. Quataert³⁴, M. Sako³, M. Sauseda¹⁰, D. J. Schlegel³⁵, L. F. Secco³, N. Smith³⁶, F. Sobreira^{37,38}, A. Stebbins¹, V. A. Villar⁷, A. K. Vivas³⁹, W. Wester¹, P. K. G. Williams⁷, B. Yanny¹, A. Zenteno³⁹, T. M. C. Abbott³⁹, F. B. Abdalla^{23,40}, K. Bechtol¹¹, A. Benoit-Lévy^{41,23,42}, E. Bertin^{41,42}, S. L. Bridle⁴³, D. Brooks²³, E. Buckley-Geer¹, D. L. Burke^{44,19}, A. Carnero Rosell^{38,45}, M. Carrasco Kind^{20,21}, J. Carretero⁴⁶, F. J. Castander⁴⁷, C. E. Cunha⁴⁴, C. B. D'Andrea³, L. N. da Costa^{38,45}, C. Davis⁴⁴, D. L. DePoy¹⁰, S. Desai⁴⁸, J. P. Dietrich^{49,50}, J. Estrada¹, E. Fernandez⁴⁶, B. Flaugher¹, P. Fosalba⁴⁷, E. Gaztanaga⁴⁷, D. W. Gerdes^{51,25}, T. Giannantonio^{52,53,54}, D. A. Goldstein^{55,33}, D. Gruen^{44,19}, G. Gutierrez¹, W. G. Hartley^{23,24}, K. Honscheid^{56,57}, B. Jain³, D. J. James⁵⁸, T. Jeltema⁵⁹, M. W. G. Johnson²¹, S. Kent^{1,4}, E. Krause⁴⁴, R. Kron^{1,4}, K. Kuehn⁶⁰, S. Kuhlmann⁶¹, N. Kuropatkin¹, O. Lahav²³, M. Lima^{62,38}, M. A. G. Maia^{38,45}, M. March³, C. J. Miller^{51,25}, R. Miquel^{63,46}, E. Neilsen¹, B. Nord¹, R. L. C. Ogando^{38,45}, A. A. Plazas⁶⁴, A. K. Romer⁶⁵, A. Roodman^{44,19}, E. S. Rykoff^{44,19}, E. Sanchez⁶⁶, V. Scarpine¹, M. Schubnell²⁵, I. Sevilla-Noarbe⁶⁶, M. Smith⁶⁷, R. C. Smith³⁹, E. Suchyta⁶⁸, G. Tarle²⁵, D. Thomas⁶⁹, R. C. Thomas³³, M. A. Troxel^{56,57}, D. L. Tucker¹, V. Vikram⁶¹, A. R. Walker³⁹, J. Weller^{49,70,54} & Y. Zhang¹

¹Fermi National Accelerator Laboratory, PO Box 500, Batavia, Illinois 60510, USA.

²Department of Physics, Brandeis University, Waltham, Massachusetts, USA.

³Department of Physics and Astronomy, University of Pennsylvania, Philadelphia, Pennsylvania 19104, USA. ⁴Kavli Institute for Cosmological Physics, University of Chicago, Chicago, Illinois 60637, USA. ⁵Harvard-Smithsonian Center for Astrophysics, 60 Garden Street, Cambridge, Massachusetts 02138, USA. ⁶Department of Physics, University of Surrey, Guildford GU2 7XH, UK. ⁷Harvard-Smithsonian Center for Astrophysics, 60 Garden Street, Cambridge, Massachusetts 02138, USA. ⁸Department of Astronomy, Indiana University, 727 East Third Street, Bloomington, Indiana 47405, USA. ⁹Astrophysical Institute, Department of Physics and Astronomy, 251B Clippinger Lab, Ohio University, Athens, Ohio 45701, USA. ¹⁰George P. and Cynthia Woods Mitchell Institute for Fundamental Physics and Astronomy, and Department of Physics and Astronomy, Texas

A&M University, College Station, Texas 77843, USA. ¹¹LSST, 933 North Cherry Avenue, Tucson, Arizona 85721, USA. ¹²Hubble and Carnegie-Dunlap Fellow. ¹³The Observatories of the Carnegie Institution for Science, 813 Santa Barbara Street, Pasadena, California 91101, USA. ¹⁴Institut d'Astrophysique de Paris (UMR7095: CNRS and UPMC), 98 bis Bd Arago, F-75014 Paris, France. ¹⁵Center for Interdisciplinary Exploration and Research in Astrophysics (CIERA) and Department of Physics and Astronomy, Northwestern University, Evanston, Illinois 60208, USA. ¹⁶Hubble Fellow. ¹⁷Center for Theoretical Astrophysics, Los Alamos National Laboratory, Los Alamos, New Mexico 87544. ¹⁸Instituto de Física Teórica UAM/CSIC, Universidad Autónoma de Madrid, 28049 Madrid, Spain. ¹⁹SLAC National Accelerator Laboratory, Menlo Park, California 94025, USA. ²⁰Department of Astronomy, University of Illinois, 1002 West Green Street, Urbana, Illinois 61801, USA. ²¹National Center for Supercomputing Applications, 1205 West Clark Street, Urbana, Illinois 61801, USA. ²²Department of Physics and Astronomy and Astrophysics, The Pennsylvania State University, University Park, Pennsylvania 16802, USA. ²³Department of Physics and Astronomy, University College London, Gower Street, London WC1E 6BT, UK. ²⁴Department of Physics, ETH Zurich, Wolfgang-Pauli-Strasse 16, CH-8093 Zurich, Switzerland. ²⁵Department of Physics, University of Michigan, Ann Arbor, Michigan 48109, USA. ²⁶Departments of Physics and Astronomy, and Theoretical Astrophysics Center, University of California, Berkeley, California 94720-7300, USA. ²⁷Observatório do Valongo, Universidade Federal do Rio de Janeiro, Ladeira do Pedro Antônio 43, Rio de Janeiro, RJ 20080-090, Brazil. ²⁸Center for Interdisciplinary Exploration and Research in Astrophysics (CIERA) and Department of Physics and Astronomy, Northwestern University, Evanston, Illinois 60208, USA. ²⁹National Optical Astronomy Observatory, 950 North Cherry Avenue, Tucson, Arizona 85719, USA. ³⁰Departamento de Astronomía, Universidad de Chile, Camino del Observatorio 1515, Las Condes, Santiago, Chile. ³¹Department of Physics and Columbia Astrophysics Laboratory, Columbia University, New York, New York 10027, USA. ³²Department of Physics, University of Michigan, 450 Church Street, Ann Arbor, Michigan 48109-1040, USA. ³³Lawrence Berkeley National Laboratory, 1 Cyclotron Road, Berkeley, California 94720, USA. ³⁴Department of Astronomy and Theoretical Astrophysics Center, University of California, Berkeley, California 94720-3411, USA. ³⁵Physics Division, Lawrence Berkeley National Laboratory, Berkeley, California 94720-8160, USA. ³⁶Steward Observatory, University of Arizona, 933 North Cherry Avenue, Tucson, Arizona 85721, USA. ³⁷Instituto de Física Gleb Wataghin, Universidade Estadual de Campinas, Campinas SP 13083-859, Brazil. ³⁸Laboratório Interinstitucional de e-Astronomia — LineA, Rua Gal. José Cristino 77, Rio de Janeiro, RJ 20921-400, Brazil. ³⁹Cerro Tololo Inter-American Observatory, National Optical Astronomy Observatory, Casilla 603, La Serena, Chile. ⁴⁰Department of Physics and Electronics, Rhodes University, PO Box 94, Grahamstown 6140, South Africa. ⁴¹CNRS, UMR 7095, Institut d'Astrophysique de Paris, F-75014 Paris, France. ⁴²Sorbonne Universités, UPMC Université Paris 06, UMR 7095, Institut d'Astrophysique de Paris, F-75014 Paris, France. ⁴³Jodrell Bank Center for Astrophysics, School of Physics and Astronomy, University of Manchester, Oxford Road, Manchester M13 9PL, UK. ⁴⁴Kavli Institute for Particle Astrophysics and Cosmology, PO Box 2450, Stanford University, Stanford, California 94305, USA. ⁴⁵Observatório Nacional, Rua Gal. José Cristino 77, Rio de Janeiro, RJ 20921-400, Brazil. ⁴⁶Institut de Física d'Altes Energies (IFAE), The Barcelona Institute of Science and Technology, Campus UAB, 08193 Bellaterra, Spain. ⁴⁷Institute of Space Sciences, IEEC-CSIC, Campus UAB, Carrer de Can Magrans, 08193 Barcelona, Spain. ⁴⁸Department of Physics, IIT Hyderabad, Kandi, Telangana 502285, India. ⁴⁹Excellence Cluster Universe, Boltzmannstrasse 2, 85748 Garching, Germany. ⁵⁰Faculty of Physics, Ludwig-Maximilians-Universität, Scheinerstrasse 1, 81679 Munich, Germany. ⁵¹Department of Astronomy, University of Michigan, Ann Arbor, Michigan 48109, USA. ⁵²Institute of Astronomy, University of Cambridge, Madingley Road, Cambridge CB3 0HA, UK. ⁵³Kavli Institute for Cosmology, University of Cambridge, Madingley Road, Cambridge CB3 0HA, UK. ⁵⁴Universitäts-Sternwarte, Fakultät für Physik, Ludwig-Maximilians-Universität München, Scheinerstrasse 1, 81679 München, Germany. ⁵⁵Department of Astronomy, University of California, Berkeley, 501 Campbell Hall, Berkeley, California 94720, USA. ⁵⁶Center for Cosmology and Astro-Particle Physics, The Ohio State University, Columbus, Ohio 43210, USA. ⁵⁷Department of Physics, The Ohio State University, Columbus, Ohio 43210, USA. ⁵⁸Astronomy Department, University of Washington, Box 351580, Seattle, Washington 98195, USA. ⁵⁹Santa Cruz Institute for Particle Physics, Santa Cruz, California 95064, USA. ⁶⁰Australian Astronomical Observatory, North Ryde, New South Wales 2113, Australia. ⁶¹Argonne National Laboratory, 9700 South Cass Avenue, Lemont, Illinois 60439, USA. ⁶²Departamento de Física Matemática, Instituto de Física, Universidade de São Paulo, CP 66318, São Paulo, SP 05314-970, Brazil. ⁶³Institució Catalana de Recerca i Estudis Avançats, E-08010 Barcelona, Spain. ⁶⁴Jet Propulsion Laboratory, California Institute of Technology, 4800 Oak Grove Drive, Pasadena, California 91109, USA. ⁶⁵Department of Physics and Astronomy, Pevensey Building, University of Sussex, Brighton BN1 9QH, UK. ⁶⁶Centro de Investigaciones Energéticas, Medioambientales y Tecnológicas (CIEMAT), Madrid, Spain. ⁶⁷School of Physics and Astronomy, University of Southampton, Southampton SO17 1BJ, UK. ⁶⁸Computer Science and Mathematics Division, Oak Ridge National Laboratory, Oak Ridge, Tennessee 37831. ⁶⁹Institute of Cosmology and Gravitation, University of Portsmouth, Portsmouth PO1 3FX, UK. ⁷⁰Max Planck Institute for Extraterrestrial Physics, Giessenbachstrasse, 85748 Garching, Germany.

The DLT40 Collaboration

J. B. Haislip¹, V. V. Kouprianov¹, D. E. Reichart¹, L. Tartaglia^{2,3}, D. J. Sand², S. Valenti³ & S. Yang^{3,4,5}

¹Department of Physics and Astronomy, University of North Carolina at Chapel Hill, Chapel Hill, North Carolina 27599, USA. ²Department of Astronomy and Steward Observatory, University of Arizona, 933 North Cherry Ave, Tucson, Arizona 85719, USA.

³Department of Physics, University of California, 1 Shields Avenue, Davis, California 95616-5270, USA. ⁴Department of Physics and Astronomy, University of Padova, Via 8 Febbraio, 2-35122 Padova, Italy. ⁵INAF Osservatorio Astronomico di Padova, Vicolo della Osservatorio 5, I-35122 Padova, Italy.

The Las Cumbres Observatory Collaboration

Iair Arcavi^{1,2}, Griffin Hosseinzadeh^{1,2}, D. Andrew Howell^{1,2}, Curtis McCully^{1,2}, Dovi Poznanski³ & Sergiy Vasylyev^{1,2}

¹Department of Physics, University of California, Santa Barbara, California 93106-9530, USA. ²Las Cumbres Observatory, 6740 Cortona Drive, Suite 102, Goleta, California 93117-5575, USA. ³School of Physics and Astronomy, Tel Aviv University, Tel Aviv 69978, Israel.

The VINROUGE Collaboration

N. R. Tanvir¹, A. J. Levan², J. Hjorth³, Z. Cano⁴, C. Copperwheat⁵, A. de Ugarte-Postigo⁴, P. A. Evans¹, J. P. U. Fynbo³, C. González-Fernández⁶, J. Greiner⁷, M. Irwin⁶, J. Lyman², I. Mandel⁸, R. McMahon⁶, B. Milvang-Jensen³, P. O'Brien¹, J. P. Osborne¹, D. A. Perley⁵, E. Pian⁹, E. Palazzi⁹, E. Rol¹⁰, S. Rosetti¹, S. Rosswog¹¹, A. Rowlinson^{12,13}, S. Schulze¹⁴, D. T. H. Steeghs², C. C. Thöne⁴, K. Ulaczyk², D. Watson³ & K. Wiersema^{1,2}

¹Department of Physics and Astronomy, University of Leicester, University Road, Leicester LE1 7RH, UK. ²Department of Physics, University of Warwick, Coventry CV4 7AL, UK. ³DARK, Niels Bohr Institute, University of Copenhagen, Juliane Maries Vej 30, 2100 Copenhagen Ø, Denmark. ⁴Instituto de Astrofísica de Andalucía (IAA-CSIC), Glorieta de la Astronomía, 18008 Granada, Spain. ⁵Astrophysics Research Institute, Liverpool John Moores University, IC2, Liverpool Science Park, 146 Brownlow Hill, Liverpool L3

5RF, UK. ⁶Institute of Astronomy, University of Cambridge, Madingley Road, Cambridge CB3 0HA, UK. ⁷Max-Planck-Institut für extraterrestrische Physik, 85740 Garching, Gießenbachstrasse 1, Germany. ⁸Birmingham Institute for Gravitational Wave Astronomy and School of Physics and Astronomy, University of Birmingham, Birmingham B15 2TT, UK. ⁹INAF, Institute of Space Astrophysics and Cosmic Physics, Via Gobetti 101, I-40129 Bologna, Italy. ¹⁰School of Physics and Astronomy, and Monash Centre for Astrophysics, Monash University, Clayton, Victoria 3800, Australia. ¹¹The Oskar Klein Centre, Department of Astronomy, AlbaNova, Stockholm University, SE-106 91 Stockholm, Sweden. ¹²Anton Pannekoek Institute, University of Amsterdam, Science Park 904, 1098 XH Amsterdam, The Netherlands. ¹³ASTRON, the Netherlands Institute for Radio Astronomy, Postbus 2, 7990 AA Dwingeloo, The Netherlands. ¹⁴Department of Particle Physics and Astrophysics, Weizmann Institute of Science, 76100 Rehovot, Israel.

The MASTER Collaboration

V. M. Lipunov^{1,2}, E. Gorbovskey², V. G. Kornilov^{1,2}, N. Tyurina², P. Balanutsa², D. Vlasenko^{1,2}, I. Gorbunov², R. Podesta³, H. Levato⁴, C. Saffe⁴, D. A. H. Buckley⁵, N. M. Budnev⁶, O. Gress^{6,2}, V. Yurkov⁷, R. Rebolo⁸ & M. Serra-Ricart⁸

¹M. V. Lomonosov Moscow State University, Physics Department, Leninskie gory, GSP-1, Moscow 119991, Russia. ²M. V. Lomonosov Moscow State University, Sternberg Astronomical Institute, Universitetsky pr., 13, Moscow 119234, Russia. ³Osservatorio Astronomico Felix Aguilar (OAFa), National University of San Juan, San Juan, Argentina. ⁴Instituto de Ciencias Astronómicas, de la Tierra y del Espacio (ICATE), San Juan, Argentina. ⁵South African Astrophysical Observatory, PO Box 9, 7935 Observatory, Cape Town, South Africa. ⁶Irkutsk State University, Applied Physics Institute, 20 Gagarin boulevard, 664003 Irkutsk, Russia. ⁷Blagoveschensk State Pedagogical University, Lenin street 104, Amur Region, Blagoveschensk 675000, Russia. ⁸Instituto de Astrofísica de Canarias Via Lactea, E-38205 La Laguna, Spain.

METHODS

Probability of optical counterpart association with NGC 4993. We calculate the probability that an NGC 4993-like galaxy (or brighter) is misidentified as the host by asking how often the centre of one or more such galaxies falls by random chance within a given angular radius θ of the counterpart. Assuming Poisson counting statistics this probability is given by $P = 1 - \exp[-\pi\theta^2 S(<m)]$ where $S(<m)$ is the surface density of galaxies with apparent magnitude equal to or brighter than m . From the local galaxy sample distribution in the infrared (K-band) apparent magnitude³⁴ we obtain $S(<K) = 0.68 \times 10^{(0.64(K-10.0)-0.7)} \text{ deg}^{-2}$. As suggested by³⁵, we set θ equal to twice the half-light radius of the galaxy, for which we use NGC 4993's diameter of about 1.1 arcmin, as measured in the near infrared band (the predominant emission band for early-type galaxies). Using $K = 9.2$ mag taken from the 2MASS survey³⁶ for NGC 4993, we find the probability of random chance association is $P = 0.004\%$.

Finding the Hubble velocity of NGC 4993. In previous electromagnetic determinations of the cosmic 'distance ladder', the Hubble flow velocity of the local calibrating galaxies has generally been estimated using redshift-independent secondary galaxy distance indicators, such as the Tully-Fisher relation or type Ia supernovae, calibrated with more distant samples that can be assumed to sit in quiet Hubble flow¹⁹. We do not adopt this approach for NGC 4993, however, in order that our inference of the Hubble constant is fully independent of the electromagnetic distance scale. Instead we estimate the Hubble flow velocity at the position of NGC 4993 by correcting its measured recessional velocity for local peculiar motions.

NGC 4993 resides in a group of galaxies whose center-of-mass recession velocity relative to the CMB frame²⁷ is²⁸ $3,327 \pm 72 \text{ km s}^{-1}$. We assume that all of the galaxies in the group are at the same distance and therefore have the same Hubble flow velocity, which we assign to be the Hubble velocity of GW170817. This assumption is accurate to within 1% given that the radius of the group is approximately 0.4 Mpc. To calculate the Hubble flow velocity of the group, we correct its measured recessional velocity by the peculiar velocity caused by the local gravitational field. This is a significant correction^{29,30}; typical peculiar velocities are 300 km s^{-1} , equivalent to about 10% of the total recessional velocity at a distance of 40 Mpc.

We employ the 6dF galaxy redshift survey peculiar velocity map^{29,38}, which used more than 8,000 Fundamental Plane galaxies to map the peculiar velocity field in the Southern Hemisphere out to redshift $z \approx 0.055$. We weight the peculiar velocity corrections from this catalog with a Gaussian kernel centered on NGC 4993's sky position and with a width of $8h^{-1}$ Mpc; the kernel width is independent of H_0 and is equivalent to a width of 800 km s^{-1} in velocity space, typical of the widths used in the catalog itself. There are 10 galaxies in the 6dF peculiar velocity catalog within one kernel width of NGC 4993. In the CMB frame²⁷, the weighted radial component of the peculiar velocity and associated uncertainty is $\langle v_p \rangle = 310 \pm 69 \text{ km s}^{-1}$.

We verified the robustness of this peculiar velocity correction by comparing it with the velocity field reconstructed from the 2MASS redshift survey^{30,39}. This exploits the linear relationship between the peculiar velocity and mass density fields smoothed on scales larger than about $8h^{-1}$ Mpc, and the constant of proportionality can be determined by comparison with radial peculiar velocities of individual galaxies estimated from, for example, Tully-Fisher and type Ia supernovae distances. Using these reconstructed peculiar velocities, which have a larger associated uncertainty³⁰ of 150 km s^{-1} , at the position of NGC 4993 we find a Hubble velocity in the CMB frame of $v_H = 3,047 \text{ km s}^{-1}$ —in excellent agreement with the result derived using 6dF. We adopt this larger uncertainty on the peculiar velocity correction in recognition that the peculiar velocity estimated from the 6dF data may represent an imperfect model of the true bulk flow at the location of NGC 4993. For our inference of the Hubble constant we therefore use a Hubble velocity $v_H = 3,017 \pm 166 \text{ km s}^{-1}$ with 68.3% uncertainty.

Finally, while we emphasise again the independence of our Hubble constant inference from the electromagnetic distance scale, we note the consistency of our gravitational-wave distance estimate to NGC 4993 with the Tully-Fisher distance estimate derived by scaling back the Tully-Fisher relation calibrated with more distant galaxies in quiet Hubble flow²⁴. This also strongly supports the robustness of our estimate for the Hubble velocity of NGC 4993.

Summary of the model. Given observed data from a set of gravitational-wave detectors, x_{GW} , parameter estimation is used to generate a posterior on the parameters that determine the waveform of the gravitational-wave signal. Parameters are inferred within a Bayesian framework⁴⁰ by comparing strain measurements¹ in the two LIGO detectors and the Virgo detector with the gravitational waveforms expected from the inspiral of two point masses⁴¹ under general relativity. We use algorithms for removing short-lived detector noise artifacts^{1,42} and we employ approximate point-particle waveform models^{41,43,44}. We have verified that the systematic changes in the results presented here from incorporating non-point-mass (tidal) effects^{45,46} and from different data processing

methods are much smaller than the statistical uncertainties in the measurement of H_0 and the binary orbital inclination angle.

From this analysis we can obtain the parameter estimation likelihood of the observed gravitational-wave data, marginalized over all parameters characterizing the gravitational-wave signal except d and $\cos i$,

$$p(x_{\text{GW}}|d, \cos i) = \int p(x_{\text{GW}}|d, \cos i, \lambda) p(\lambda) d\lambda$$

The other waveform parameters are denoted by λ , with $p(\lambda)$ denoting the corresponding prior.

Given perfect knowledge of the Hubble flow velocity of the gravitational-wave source, v_H , this posterior distribution can be readily converted into a posterior on $\cos i$ and $H_0 = v_H/d$,

$$p(H_0, \cos i|x_{\text{GW}}) \propto (v_H/H_0^2) p(x_{\text{GW}}|d = v_H/H_0, \cos i) p_d(v_H/H_0) p_i(\cos i)$$

where $p_d(d)$ and $p_i(\cos i)$ are the prior distributions on distance and inclination. For the Hubble velocity $v_H = 3,017 \text{ km s}^{-1}$, the maximum a posteriori distance from the gravitational-wave measurement of 43.8 Mpc corresponds to $H_0 = 68.9 \text{ km s}^{-1} \text{ Mpc}^{-1}$, so this procedure would be expected to generate a posterior on H_0 that peaks close to that value.

While the above analysis is conceptually straightforward, it makes a number of assumptions. In practice, the Hubble-flow velocity cannot be determined exactly and it must be corrected for uncertain peculiar velocities. The above does not explicitly set a prior on H_0 , but instead inherits a $1/H_0^4$ prior from the usual $p_d(d) \propto d^2$ prior used in gravitational-wave parameter estimation. In addition, the logic in this model is that a redshift has been obtained first and the distance is then measured using gravitational waves. As gravitational-wave detectors cannot be pointed, we cannot target particular galaxies or redshifts for gravitational-wave sources. In practice, we wait for a gravitational-wave event to trigger the analysis and this introduces potential selection effects which we must consider. We will see below that the simple analysis described above does give results that are consistent with a more careful analysis for this first detection. However, the simple analysis cannot be readily extended to include second and subsequent detections, so we now describe a more general framework that does not suffer from these limitations.

We suppose that we have observed a gravitational-wave event, which generated data x_{GW} in our detectors, and that we have also measured a recessional velocity for the host, v_r , and the peculiar velocity field, $\langle v_p \rangle$, in the vicinity of the host. These observations are statistically independent and so the combined likelihood is

$$p(x_{\text{GW}}, v_r, \langle v_p \rangle | d, \cos i, v_p, H_0) = p(x_{\text{GW}}|d, \cos i) p(v_r|d, v_p, H_0) p(\langle v_p \rangle | v_p) \quad (2)$$

The quantity $p(v_r | d, v_p, H_0)$ is the likelihood of the recessional velocity measurement, which we model as

$$p(v_r|d, v_p, H_0) = N[v_r + H_0 d, \sigma_{v_r}^2](v_r)$$

where $N[\mu, \sigma^2](x)$ is the normal (Gaussian) probability density with mean μ and standard deviation σ evaluated at x . The measured recessional velocity, $v_r = 3,327 \text{ km s}^{-1}$, with uncertainty $\sigma_{v_r} = 72 \text{ km s}^{-1}$, is the mean velocity and standard error for the members of the group hosting NGC 4993 taken from the 2MASS²⁸, corrected to the CMB frame²⁷. We take a similar Gaussian likelihood for the measured peculiar velocity, $\langle v_p \rangle = 310 \text{ km s}^{-1}$, with uncertainty $\sigma_{v_p} = 150 \text{ km s}^{-1}$:

$$p(\langle v_p \rangle | v_p) = N[v_p, \sigma_{v_p}^2](\langle v_p \rangle)$$

From the likelihood (2) we derive the posterior

$$p(H_0, d, \cos i, v_p | x_{\text{GW}}, v_r, \langle v_p \rangle) \propto \frac{p(H_0)}{\mathcal{N}_s(H_0)} p(x_{\text{GW}}|d, \cos i) p(v_r|d, v_p, H_0) \times p(\langle v_p \rangle | v_p) p(d) p(v_p) p(\cos i) \quad (3)$$

where $p(H_0)$, $p(d)$, $p(v_p)$ and $p(\cos i)$ are the parameter prior probabilities. Our standard analysis assumes a volumetric prior, $p(d) \propto d^2$, on the Hubble distance, but we explore sensitivity to this choice below. We take a flat-in-log prior on H_0 , $p(H_0) \propto 1/H_0$, impose a flat (that is, isotropic) prior on $\cos i$, and a flat prior on v_p for $v_p \in [-1,000, 1,000] \text{ km s}^{-1}$. These priors characterise our beliefs about the cosmological population of gravitational-wave events and their hosts before we make any additional measurements or account for selection biases. The full statistical model is summarized graphically in Extended Data Fig. 1. This model with these priors is our canonical analysis.

In equation (3), the term $\mathcal{N}_s(H_0)$ encodes selection effects^{25,47,48}. These arise because of the finite sensitivity of our detectors. While all events in the Universe

generate a response in the detector, we will only be able to identify, and hence use, signals that generate a response of sufficiently high amplitude. The decision about whether to include an event in the analysis is a property of the data only, in this case $\{x_{\text{GW}}, v_p, \langle v_p \rangle\}$, but the fact that we condition our analysis on a signal being detected, that is, the data exceeding these thresholds, means that the likelihood must be renormalized to become the likelihood for detected events. This is the role of

$$\mathcal{N}_s(H_0) = \int_{\text{detectable}} [p(x_{\text{GW}}|d, \cos \iota, \lambda) p(v_r|d, v_p, H_0) p(\langle v_p \rangle|v_p) \times p(\lambda) p(d) p(v_p) p(\cos \iota)] d\lambda dd dv_p d\cos \iota dx_{\text{GW}} dv_r d\langle v_p \rangle \quad (4)$$

where the integral is over the full prior ranges of the parameters, $\{d, v_p, \cos \iota, \lambda\}$, and over data sets that would be selected for inclusion in the analysis, that is, exceed the specified thresholds. If the integral was over all data sets it would evaluate to 1, but because the range is restricted there can be a non-trivial dependence on parameters characterizing the population of sources, in this case H_0 .

In the current analysis, there are in principle selection effects in both the gravitational-wave data and the electromagnetic data. However, around the time of detection of GW170817, the LIGO–Virgo detector network had a detection horizon of approximately 190 Mpc for BNS events¹, within which electromagnetic measurements are largely complete. For example, the counterpart associated with GW170817 had brightness of about 17 mag in the I band at 40 Mpc^{26,49–52}; this source would be about 22 mag at 400 Mpc, and thus still detectable by survey telescopes such as DECam well beyond the gravitational-wave horizon. Even the dimmest theoretical lightcurves for kilonovae are expected to peak at about 22.5 mag at the LIGO–Virgo horizon⁵³. We therefore expect that we are dominated by gravitational-wave selection effects at the current time and can ignore electromagnetic selection effects. The fact that the fraction of BNS events that will have observed kilonova counterparts is presently unknown does not modify these conclusions, since we can restrict our analysis to gravitational-wave events with kilonova counterparts only.

In the gravitational-wave data, the decision about whether or not to analyse an event is largely determined by the signal-to-noise ratio, ρ , of the event. A reasonable model for the selection process is a cut in signal-to-noise ratio, that is, events with $\rho > \rho_*$ are analysed⁵⁴. In that model, the integral over x_{GW} in equation (4) can be replaced by an integral over signal-to-noise ratio from ρ_* to ∞ , and $p(x_{\text{GW}}|d, \cos \iota, \lambda)$ replaced by $p(\rho|d, \cos \iota, \lambda)$ in the integrand. This distribution depends on the noise properties of the operating detectors, and on the intrinsic strain amplitude of the source. The former are clearly independent of the population parameters, while the latter scales like a function of the source parameters divided by the luminosity distance. The dependence on source parameters is on redshifted parameters, which introduces an explicit redshift dependence. However, within the approximately 190-Mpc horizon, redshift corrections are at most less than about 5%, and the Hubble constant measurement is a weak function of these, meaning the overall impact is even smaller. At present, whether or not a particular event in the population ends up being analysed can therefore be regarded as a function of d only. When gravitational-wave selection effects dominate, only the terms in equation (4) arising from the gravitational-wave measurement matter. As these are a function of d only and we set a prior on d , there is no explicit H_0 dependence in these terms. Hence, $\mathcal{N}_s(H_0)$ is a constant and can be ignored. This would not be the case if we set a prior on the redshifts of potential sources instead of their distances, since then changes in H_0 would modify the range of detectable redshifts. As the LIGO–Virgo detectors improve in sensitivity the redshift dependence in the gravitational-wave selection effects will become more important, as will electromagnetic selection effects. However, at that point we will also have to consider deviations in the cosmological model from the simple Hubble flow described in equation (1).

Marginalizing equation (3) over d, v_p and $\cos \iota$ then yields

$$p(H_0|x_{\text{GW}}, v_r, \langle v_p \rangle) \propto p(H_0) \int [p(x_{\text{GW}}|d, \cos \iota) p(v_r|d, v_p, H_0) p(\langle v_p \rangle|v_p) \times p(d) p(v_p) p(\cos \iota)] dd dv_p d\cos \iota$$

The posterior computed in this way was shown in Fig. 1 and has a maximum a posteriori value and minimal 68.3% credible interval of $70.0_{-8.0}^{+12.0} \text{ km s}^{-1} \text{ Mpc}^{-1}$, as quoted in the main article. The posterior mean is $78 \text{ km s}^{-1} \text{ Mpc}^{-1}$ and the standard deviation is $15 \text{ km s}^{-1} \text{ Mpc}^{-1}$. Various other summary statistics are given in Extended Data Table 1.

Robustness to prior specification. Our canonical analysis uses a uniform volumetric prior on distance, $p(d) \propto d^2$. The distribution of galaxies is not completely uniform due to clustering, so we explore sensitivity to this prior choice.

We are free to place priors on any two of the three variables $\{d, H_0, z\}$, where $z = H_0/d/c$ is the Hubble flow redshift of NGC 4993. A choice of prior for two of these variables induces a prior on the third which may or may not correspond to a natural choice for that parameter. A prior on z could be obtained from galaxy catalog observations⁵⁵, but must be corrected for incompleteness. When setting a prior on H_0 and z , the posterior becomes

$$p(H_0, z, \cos \iota, v_p|x_{\text{GW}}, v_r, \langle v_p \rangle) \propto \frac{p(H_0)}{\mathcal{N}_s(H_0)} p(x_{\text{GW}}|d = cz/H_0, \cos \iota) p(v_r|z, v_p) \times p(\langle v_p \rangle|v_p) p(z) p(v_p) p(\cos \iota)$$

but now

$$\mathcal{N}_s(H_0) = \int_{\text{detectable}} [p(x_{\text{GW}}|d = cz/H_0, \cos \iota) p(v_r|z, v_p) \times p(\langle v_p \rangle|v_p) p(z) p(v_p) p(\cos \iota)] dz dv_p d\cos \iota dx_{\text{GW}} dv_r d\langle v_p \rangle$$

When gravitational-wave selection effects dominate, the integral is effectively

$$p_{\text{det}}(H_0) = \int p(x_{\text{GW}}|d = cz/H_0, \cos \iota) p(z) p(\cos \iota) dz d\cos \iota dx_{\text{GW}} = \int p(x_{\text{GW}}|d, \cos \iota) p(dH_0/c) p(\cos \iota) (H_0/c) dd d\cos \iota dx_{\text{GW}}$$

which has an H_0 dependence, unless $p(z)$ takes a special, H_0 -dependent form, $p(z) = f(z/H_0)/H_0$. However, if the redshift prior is volumetric, $p(z) \propto z^2$, the selection effect term is proportional to H_0^3 , which cancels a similar correction to the likelihood and gives a posterior on H_0 that is identical to the canonical analysis.

For a single event, any choice of prior can be mapped to our canonical analysis with a different prior on H_0 . For any reasonable prior choices on d or z , we would expect to gradually lose sensitivity to the particular prior choice as further observed events are added to the analysis. However, to illustrate the uncertainty that comes from the prior choice for this first event, we compare in Extended Data Fig. 2 and Extended Data Table 1 the results from the canonical prior choice $p(d) \propto d^2$ to those from two other choices: using a flat prior on z , and assuming a velocity correction due to the peculiar velocity of NGC 4993 that is a Gaussian with width 250 km s^{-1} . (To do the first of these, the posterior samples from gravitational-wave parameter estimation have to be re-weighted, since they are generated with the d^2 prior used in the canonical analysis. We first ‘undo’ the default prior before applying the desired new prior.)

The choice of a flat prior on z is motivated by the simple model described above, in which we imagine first making a redshift measurement for the host and then use that as a prior for analysing the gravitational-wave data. Setting priors on distance and redshift, the simple analysis gives the same result as the canonical analysis, but now we set a prior on redshift and H_0 and obtain a different result. This is to be expected because we are making different assumptions about the underlying population, and it arises for similar reasons as the different biases in peculiar velocity measurements based on redshift-selected or distance-selected samples⁵⁶. As can be seen in Extended Data Table 1, the results change by less than 1σ , as measured by the statistical error of the canonical analysis.

By increasing the uncertainty in the peculiar velocity prior, we test the assumptions in our canonical analysis that (1) NGC 4993 is a member of the nearby group of galaxies, and (2) that this group has a center-of-mass velocity close to the Hubble flow. The results in Extended Data Table 1 summarizes changes in the values of H_0 and in the error bars.

We conclude that the impact of a reasonable change to the prior is small relative to the statistical uncertainties for this event.

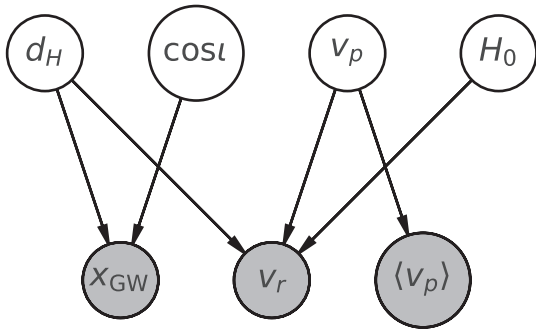
Incorporating additional constraints on H_0 . By including previous measurements of H_0 (refs 20, 21) we can constrain the orbital inclination more precisely. We do this by setting the H_0 prior in equation (3) to $p(H_0|\mu_{H_0}, \sigma_{H_0}^2) = N[\mu_{H_0}, \sigma_{H_0}^2]$, where for ShoES²¹ $\mu_{H_0} = 73.24 \text{ km s}^{-1} \text{ Mpc}^{-1}$ and $\sigma_{H_0} = 1.74 \text{ km s}^{-1} \text{ Mpc}^{-1}$, while for Planck²⁰ $\mu_{H_0} = 67.74 \text{ km s}^{-1} \text{ Mpc}^{-1}$ and $\sigma_{H_0} = 0.46 \text{ km s}^{-1} \text{ Mpc}^{-1}$. The posterior on $\cos \iota$ is then

$$p(\cos \iota|x_{\text{GW}}, v_r, \langle v_p \rangle, \mu_{H_0}, \sigma_{H_0}^2) \propto \int [p(x_{\text{GW}}|d, \cos \iota) p(v_r|d, v_p, H_0) p(\langle v_p \rangle|v_p) \times p(H_0|\mu_{H_0}, \sigma_{H_0}^2) p(d) p(v_p)] dd dv_p dH_0$$

This posterior is shown in Fig. 3.

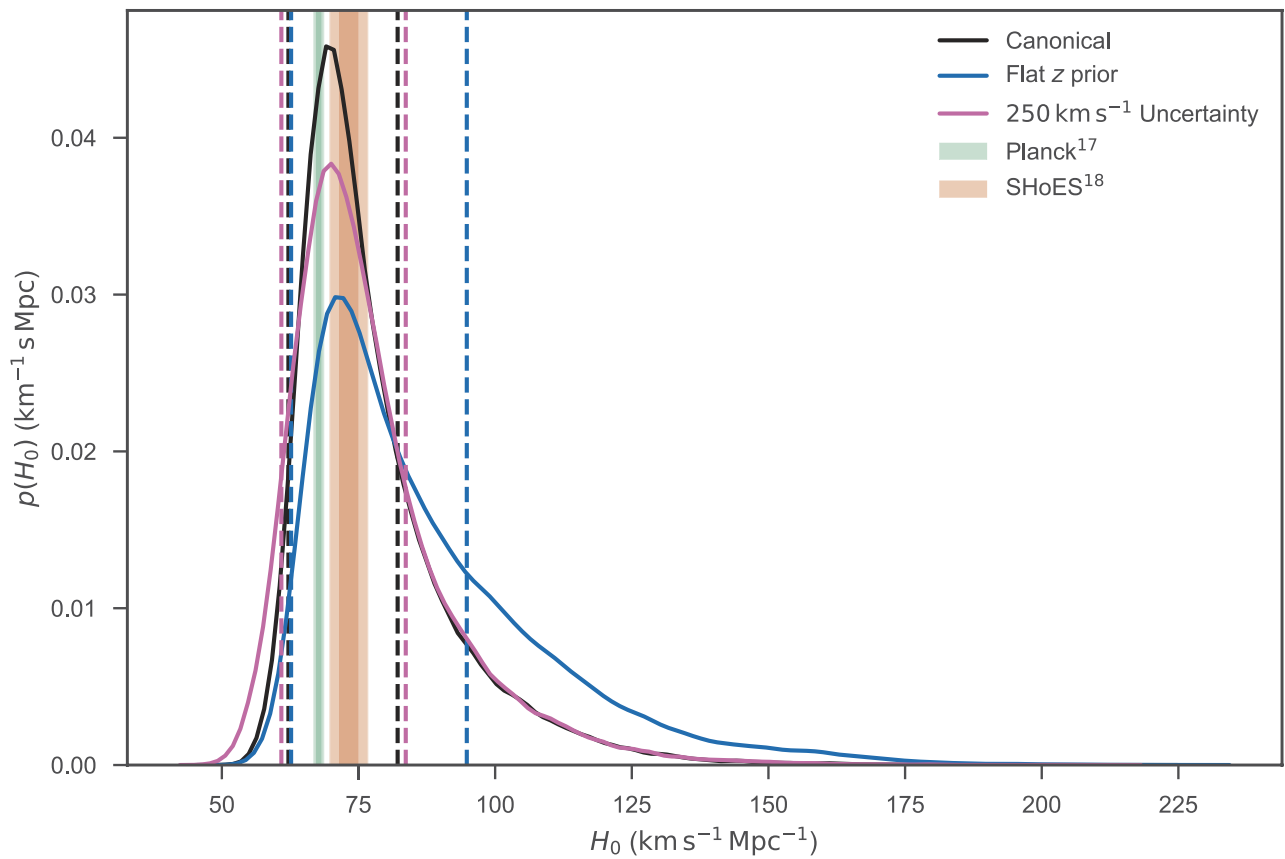
Data and code availability. The publicly available codes and data can be found at the LIGO Open Science Center (<https://losc.ligo.org>).

34. Huang, J.-S., Cowie, L. L. & Luppino, G. A. Morphological classification of the local I- and K-band galaxy sample. *Astrophys. J.* **496**, 31–38 (1998).
35. Bloom, J. S., Kulkarni, S. R. & Djorgovski, S. G. The observed offset distribution of gamma-ray bursts from their host galaxies: a robust clue to the nature of the progenitors. *Astron. J.* **123**, 1111–1148 (2002).
36. Skrutskie, M. F. *et al.* The Two Micron All Sky Survey (2MASS). *Astron. J.* **131**, 1163–1183 (2006).
38. Jones, D. H. *et al.* The 6dF Galaxy Survey: final redshift release (DR3) and southern large-scale structures. *Mon. Not. R. Astron. Soc.* **399**, 683–698 (2009).
39. Huchra, J. P. *et al.* The 2MASS Redshift Survey—description and data release. *Astrophys. J. Suppl. Ser.* **199**, 26 (2012).
40. Veitch, J. *et al.* Parameter estimation for compact binaries with ground-based gravitational-wave observations using the LALInference software library. *Phys. Rev. D* **91**, 042003 (2015).
41. Hannam, M. *et al.* Simple model of complete precessing black-hole-binary gravitational waveforms. *Phys. Rev. Lett.* **113**, 151101 (2014).
42. Cornish, N. J. & Littenberg, T. B. Bayeswave: Bayesian inference for gravitational wave bursts and instrument glitches. *Class. Quantum Gravity* **32**, 135012 (2015).
43. Buonanno, A. & Damour, T. Effective one-body approach to general relativistic two-body dynamics. *Phys. Rev. D* **59**, 084006 (1999).
44. Blanchet, L. Gravitational radiation from post-Newtonian sources and inspiralling compact binaries. *Living Rev. Relativ.* **17**, 2 (2014).
45. Hinderer, T. & Flanagan, É. É. Two-timescale analysis of extreme mass ratio inspirals in Kerr spacetime: orbital motion. *Phys. Rev. D* **78**, 064028 (2008).
46. Vines, J., Flanagan, É. É. & Hinderer, T. Post-1-Newtonian tidal effects in the gravitational waveform from binary inspirals. *Phys. Rev. D* **83**, 084051 (2011).
47. Loredó, T. J. Accounting for source uncertainties in analyses of astronomical survey data. *AIP Conf. Proc.* **735**, 195–206 (2004).
48. Mandel, I., Farr, W. M. & Gair, J. Extracting distribution parameters from multiple uncertain observations with selection biases. Report No. P1600187-v1, <https://dcc.ligo.org/LIGO-P1600187/public> (LIGO, 2016).
49. Valenti, S. LIGO/Virgo g298048: Dlt40 optical candidate. GCN 21531 (2017).
50. Arcavi, I. *et al.* LIGO/Virgo g298048: galaxy-targeted optical followup with Las Cumbres Observatory. GCN 21543 (2017).
51. Tanvir, N. R. *et al.* LIGO/Virgo g298048: Vista/vircam detection of candidate counterpart. GCN 21544 (2017).
52. Coulter, D. A. *et al.* LIGO/Virgo g298048: correction to swope photometry announced in LVC GCN 21529. GCN 21567 (2017).
53. Metzger, B. D. & Berger, E. What is the most promising electromagnetic counterpart of a neutron star binary merger? *Astrophys. J.* **746**, 48 (2012).
54. Abbott, B. P. *et al.* Supplement: “The rate of binary black hole mergers inferred from Advanced LIGO observations surrounding GW150914” (2016, ApJL, 833, L1). *Astrophys. J. Suppl. Ser.* **227**, 14 (2016).
55. Dalya, G., Frei, Z., Galgoczi, G., Raffai, P. & de Souza, R. S. GLADE catalog (Dalya+, 2016). *VizieR Online Data Catalog* <http://vizier.u-strasbg.fr/viz-bin/VizieR?source=VII/275> (2016).
56. Strauss, M. A. & Willick, J. A. The density and peculiar velocity fields of nearby galaxies. *Phys. Rep.* **261**, 271–431 (1995).



Extended Data Figure 1 | Graphical model illustrating the statistical relationships between the data and parameters. Open circles indicate parameters which require a prior; filled circles described measured data, which are conditioned on in the analysis. Here we assume we have measurements of the gravitational-wave data, x_{GW} , a recession velocity (that is, redshift), v_r , and the mean peculiar velocity in the neighborhood of NGC 4993, $\langle v_p \rangle$. Arrows flowing into a node indicate that the conditional probability density for the node depends on the source parameters; for example, the conditional distribution for the observed gravitational-wave data, $p(x_{\text{GW}} | d, \cos i)$, discussed in the text, depends on the distance and inclination of the source (and additional parameters, here marginalized out).

ACCELERATED ARTICLE PREVIEW



Extended Data Figure 2 | Using different assumptions compared to our canonical analysis. The posterior distribution on H_0 discussed in the main text is shown in black, the alternative flat prior on z (discussed in Methods) gives the distribution shown in blue, and the increased

uncertainty (250 km s^{-1}) applied to our peculiar velocity measurement (also discussed in Methods) is shown in pink. Minimal 68.3% (1σ) credible intervals are shown by dashed lines.

Extended Data Table 1 | Summary of constraints on the Hubble constant, binary inclination and distance

Parameter	68.3% Symm.	68.3% MAP	90% Symm.	90% MAP
$H_0/$ (km s ⁻¹ Mpc ⁻¹)	74.0 ^{+16.0} _{-8.0}	70.0 ^{+12.0} _{-8.0}	74.0 ⁺³³ ₋₁₂	70.0 ⁺²⁸ ₋₁₁
$H_0/$ (km s ⁻¹ Mpc ⁻¹) (flat in z prior)	81 ⁺²⁷ ₋₁₃	71.0 ^{+23.0} _{-9.0}	81 ⁺⁵⁰ ₋₁₇	71.0 ⁺⁴⁸ ₋₁₁
$H_0/$ (km s ⁻¹ Mpc ⁻¹) (250 km s ⁻¹ σ_{v_r})	74.0 ^{+16.0} _{-9.0}	70.0 ^{+14.0} _{-9.0}	74.0 ⁺³³ ₋₁₄	70.0 ⁺²⁹ ₋₁₄
$\cos \iota$ (GW only)	-0.88 ^{+0.18} _{-0.09}	-0.974 ^{+0.164} _{-0.026}	-0.88 ^{+0.32} _{-0.11}	-0.974 ^{+0.332} _{-0.026}
$\cos \iota$ (SHoES)	-0.901 ^{+0.065} _{-0.057}	-0.912 ^{+0.061} _{-0.059}	-0.901 ^{+0.106} _{-0.083}	-0.912 ^{+0.095} _{-0.086}
$\cos \iota$ (Planck)	-0.948 ^{+0.052} _{-0.036}	-0.982 ^{+0.060} _{-0.016}	-0.948 ^{+0.091} _{-0.046}	-0.982 ^{+0.104} _{-0.018}
ι /deg (GW only)	152 ⁺¹⁴ ₋₁₇	167 ⁺¹³ ₋₂₃	152 ⁺²⁰ ₋₂₇	167 ⁺¹³ ₋₃₇
ι /deg (SHoES)	154.0 ^{+9.0} _{-8.0}	156.0 ^{+10.0} _{-7.0}	154.0 ⁺¹⁵ ₋₁₂	156.0 ⁺²¹ ₋₁₁
ι /deg (Planck)	161.0 ^{+8.0} _{-8.0}	169.0 ^{+8.0} _{-12.0}	161.0 ⁺¹² ₋₁₂	169.0 ⁺¹¹ ₋₁₈
$d/$ (Mpc)	41.1 ^{+4.0} _{-7.3}	43.8 ^{+2.9} _{-6.9}	41.1 ^{+5.6} _{-12.6}	43.8 ^{+5.6} _{-13.1}

We give both 1 σ (68.3%) and 90% credible intervals for each quantity. 'Symm' refers to a symmetric interval (for example, median and 5% to 95% range), while 'MAP' refers to maximum a posteriori intervals (for example, MAP value and smallest range enclosing 90% of the posterior). Values given for ι are derived from arccosine transforming the corresponding values for $\cos \iota$, so the 'MAP' values differ from those that would be derived from the posterior on ι .